

STRUCTURE-PROPERTY-PROCESSING ANALYSIS OF GRAPHENE
BIOSCAFFOLDS FOR VIABILITY AND DIFFERENTIATION OF C2C12 CELLS

by

Lynn Karriem



A thesis

submitted in partial fulfillment

of the requirements for the degree of

Master of Science in Materials Science and Engineering

Boise State University

May 2023

© 2023

Lynn Karriem

ALL RIGHTS RESERVED

BOISE STATE UNIVERSITY GRADUATE COLLEGE

DEFENSE COMMITTEE AND FINAL READING APPROVALS

of the thesis submitted by

Lynn Karriem

Thesis Title: Structure-Property-Processing Analysis of Graphene Bioscaffolds for Viability and Differentiation of C2C12 Cells

Date of Final Oral Examination: 03 February 2023

The following individuals read and discussed the thesis submitted by student Lynn Karriem, and they evaluated the student's presentation and response to questions during the final oral examination. They found that the student passed the final oral examination.

David Estrada, Ph.D.

Chair, Supervisory Committee

Julia Oxford, Ph.D.

Member, Supervisory Committee

Amy Moll, Ph.D.

Member, Supervisory Committee

The final reading approval of the thesis was granted by David Estrada, Ph.D., Chair of the Supervisory Committee. The thesis was approved by the Graduate College.

DEDICATION

This work is dedicated to my family and friends who have provided me with love and support for all these years. I wouldn't have made it this far without each and every one of you.

ACKNOWLEDGMENTS

I would like to thank my thesis advisors, Dr. Estrada, Dr. Oxford, and Dr. Moll for their guidance, mentorship, and advocacy throughout my academic career. A special thanks to Jessica Economy and the rest of the Materials Science and Engineering admin staff. Thank you all for creating a warm and supportive environment to come to on the days that were difficult. This research was kindly supported by NIGMS under P20GM103408 and P20GM109095 and NSF under 0619793 and 0923535.

ABSTRACT

We investigated the structure – property – processing correlation of graphene bioscaffolds produced using three different methods. Bioscaffolds were prepared by chemical vapor deposition (CVD), sublimation of Silicon Carbide (SiC), and printed solvent assisted exfoliated graphene ink. To gain insight into the roughness and topography of graphene, AFM was performed on each bioscaffold. Raman spectroscopy mapping demonstrated differences in the I_{2D}/I_G ratio for each scaffold. Young's modulus was determined by nanoindentation and indicated that epitaxial graphene had the highest average stiffness, followed by CVD, with printed graphene demonstrating the lowest average stiffness. To investigate the biocompatibility of each scaffold, cellular morphology and gene expression patterns were investigated using the bipotential mouse C2C12 cell line. While it is well established that cell differentiation is influenced by the structure and mechanical properties of the substratum to which cells are attached, this study provides new information about differences in cellular response to graphene scaffolds prepared by specific production methods. Graphene production methods determine the structural and mechanical properties of the resulting bioscaffold, which in turn determine cell morphology, gene expression patterns and cell differentiation fate. Therefore, production methods for graphene bioscaffolds must be chosen carefully with the ultimate biomedical application in mind.

TABLE OF CONTENTS

DEDICATION	iv
ACKNOWLEDGMENTS	v
ABSTRACT	vi
LIST OF TABLES	ix
LIST OF FIGURES	x
LIST OF ABBREVIATIONS	xii
CHAPTER ONE: INTRODUCTION	1
1.1 Motivation.....	1
1.2 Research Goals.....	2
CHAPTER TWO: BACKGROUND.....	6
2.1 Graphene.....	6
2.2 Graphene Synthesis	8
2.3 Graphene characterization	10
Atomic force microscopy (AFM) and Nanoindentation.....	10
Raman spectroscopy	11
2.4 Graphene-based bioscaffolds.....	12
2.5 The Musculoskeletal System	15
2.6 Skeletal muscle composition, structure and function.....	17
2.7 C2C12 cells.....	20

CHAPTER THREE: MANUSCRIPT	21
3.1 Abstract	21
3.2 Introduction	22
3.3 Results.....	25
Graphene Characterization	25
Cell Growth and Morphology.....	27
Assessment of differential gene expression of differential markers.....	30
Genetic Expression Profiles	31
3.4 Discussion	34
3.5 Conclusion.....	36
3.6 Methods.....	36
Chemical vapor deposition (CVD) Graphene film growth and transfer ...	36
Graphene Ink Synthesis and Printing.....	37
Epitaxial Graphene Growth on SiC	38
Materials Characterization.....	38
qPCR	40
3.7 Supporting figures and tables	42
CHAPTER 4: CONCLUSION	50
4.1 Summary	50
4.2 Limitations	51
4.3 Future work.....	53
REFERENCES	54

LIST OF TABLES

Table 2.1	Graphene bioscaffolds used in musculoskeletal tissue engineering.....	14
Table 3.1	Genes relating to myogenesis	45
Table 3.2	Genes relating to contractility	46
Table 3.3	Genes relating to the ECM.....	47
Table 3.4	Genes relating to attachment.....	48
Table 3.5	Genes relating to ECM remodeling.....	49

LIST OF FIGURES

Figure 1.1	Graphene-cell interactions.....	4
Figure 1.2	Brief outline of experimental methods highlighting, 1) graphene bioscaffold synthesis methods, 2) cell culture methods, and 3) characterization methods performed for cells on the bioscaffolds	5
Figure 2.1	Structure of graphene and graphene derivatives a) monolayer graphene, b) few-layer graphene, c) graphite, d) reduced graphene oxide (rGO), and e) graphene oxide (GO).....	7
Figure 2.2	Graphene synthesis methods, a) micromechanical exfoliation, b) liquid phase exfoliation, c) epitaxial graphene on SiC, and d) chemical vapor deposition ³⁴	9
Figure 2.3	The musculoskeletal system can be split into two parts, a) skeletal bone (left) and skeletal muscle (right). Joints (labeled by body part) are formed by bones, cartilage, ligaments, muscle, and other connective tissues and is seen in b) which represents a close up of the knee joint. (Figure by Biorender).....	17
Figure 2.4	Components of skeletal muscle as it attaches to bone through the tendon ²	18
Figure 3.1	Schematic of the different graphene synthesis methods, cell culture outline, and the characterization techniques utilized.	24
Figure 3.2	Graphene bioscaffold characterized by AFM, Raman spectroscopy, and Nanoindentation. Structure and roughness taken by AFM for a) CVD, b) Epitaxial, and c) Printed. Raman intensity maps for 2D- and G- peak ratios for d) CVD, e) Epitaxial, and f) Printed. Nanoindentation histograms representing bioscaffold stiffness for g) CVD, h) Epitaxial, and Printed. (AFM and Raman map scale bar = 2 μ m).....	26
Figure 3.3	Calcein-AM stained C2C12 images taken by optical microscope show cell morphology was influenced by graphene bioscaffolds and control substrates. Control substrates a) Quartz, b) SiC and c) glass coverslip, and graphene bioscaffolds d) CVD, e) Epitaxial and f) Printed. (Scale bar = 300 μ m)	28

Figure 3.4	Aspect ratio and alignment studies reveal quantitative morphological differences between the graphene bioscaffolds and respective controls. Aspect ratios for a) Quartz is higher than CVD, b) Epitaxial is higher than SiC control, and c) Printed is higher than glass. Alignment analysis show more alignment in d) CVD over quartz, e) SiC over epitaxial, and f) glass over printed.	30
Figure 3.5	a) Heatmap displaying gene expression patterns seen for the three graphene bioscaffolds. b) Genes related to attachment, c) genes related to myogenesis, d) genes related to contractility, e) genes related to ECM, and f) genes related to remodeling. (Tables 3.1, 3.2, 3.3, 3.4 and 3.5 highlight gene functions)	32
Figure 3.6	2D FWHM for all graphene bioscaffolds represented in Raman spectra maps where a) is CVD, b) epitaxial, and c) printed graphene and histograms of these positions where d) is CVD, e) epitaxial, and f) printed graphene.....	42
Figure 3.7	G-peak position for all graphene bioscaffolds represented in Raman spectra maps where a) is CVD, b) epitaxial, and c) printed graphene and histograms of these positions where d) is CVD, e) epitaxial, and f) printed graphene.....	43
Figure 3.8	2D-peak position for all graphene bioscaffolds represented in Raman spectra maps where a) is CVD, b) epitaxial, and c) printed graphene and histograms of these positions where d) is CVD, e) epitaxial, and f) printed graphene.....	44

LIST OF ABBREVIATIONS

VML	Volumetric Muscle Loss
MSDs	Musculoskeletal disorders
ECM	Extracellular matrix
GF	Graphene foam
GO	Graphene oxide
rGO	Reduced graphene oxide
GNS	Graphene nanosheets
CVD	Chemical vapor deposition
LPE	Liquid-phase exfoliation
FLG	Few-layer-graphene
UHV	Ultra-high vacuum
IJP	Inkjet printer
SiC	Silicon carbide
AFM	Atomic force microscopy
FWHM	Full width half maximum
MMP	Matrix metalloproteinase
DGC	Dystrophin glycoprotein complex
PGs	Proteoglycans
BMP-2	Bone morphogenic protein-2
Ra	Roughness area

qRT-PCR	Quantitative real time – polymerase chain reaction
HKG	Housekeeping gene

CHAPTER ONE: INTRODUCTION

1.1 Motivation

Skeletal muscle, a component of the musculoskeletal system, is responsible for locomotion of the body and is comprised of approximately 40-45% of body mass, making it the most abundant tissue in the human body.^{1,2} The musculoskeletal system comprised of bones, muscle, connective tissue, cartilage, tendons, and ligaments work together to provide the human body with stability, protection of the internal organs, and movement. Our ability as humans to move about our day, performing tasks which enable us to live and thrive in life is all made possible by our musculoskeletal system. Skeletal muscle disorders such as the various forms of muscular dystrophy, atrophy of the muscle and volumetric muscle loss (VML), along with other associated musculoskeletal disorders (MSDs) (Osteoarthritis, Rheumatoid arthritis, cancers of the bone and connective tissue, and deformation of the spine) have a worldwide reach by effecting the quality of life for people.³ Traumatic injury to skeletal muscle and diseases related to skeletal muscle can lead to volumetric muscle loss (VML) which in turn can affect the ability to perform day-to-day tasks.⁴ When significant tissue loss is present, treatment options are limited because native biophysical and biochemical signaling cues are no longer available to aid in regeneration.² Interventional measures such as transplantation of intact tissue has been the method of choice to address the loss of tissue and requires donated intact tissue which is limited because the supply does not meet the demand.⁵ Tissue engineering has potential to serve as an optional treatment for restoring damaged

tissue by utilizing scaffolds, stem cells and growth factors.⁶ The tissue engineering field is faced with challenges associated with scaffold compatibility.

1.2 Research Goals

Scaffolds utilized in the regeneration and engineering of biological tissue (bioscaffolds) must be biocompatible, biodegradable, and have morphological and physical properties which enable them to mimic the microenvironment^{6,7} to support structural needs such as cell attachment and tissue development.⁷ Physical scaffolding, mechanical stability, and biochemical cues are provided by the extracellular matrix (ECM)⁷, which thereby makes the ECM an important component in tissue engineering and regeneration.

At present, many researchers have published successful results displaying graphene's performance as a bioscaffold. Produced by numerous synthesis methods, graphene, in its various forms, graphene foam (GF), graphene film, epitaxial graphene, graphene oxide (GO), and reduced graphene oxide (rGO) has shown success in bone, muscle, and neuronal tissue growth.^{8,9,10-15} Surface properties such as roughness, stiffness and other topographical features in these studies have shown to affect the cell behavior. This current study aims to assess the interrelationships between graphene processing methods, structure, and properties to determine how these aspects impact the cells grown on each type of graphene. This study seeks to contrast the behavior of C2C12 cells on graphene bioscaffolds, produced by chemical vapor deposition (CVD), epitaxial growth, and solvent assisted exfoliation.

Graphene's structure and properties are seen to be dependent on the synthesis process used, however, these studies do not directly compare the cell behavior observed based on these differences. Therefore, the thesis objectives are as follows:

- 1) Show that different graphene processing methods result in graphene bioscaffolds with different structures and properties
- 2) Show that the different structures and properties produced by the different processing methods impact how graphene performs as a bioscaffold

Direct comparisons made between graphene type and how cells are influenced by each type can expand the knowledge already gained on how graphene's properties effect cells. A greater breadth of understanding provides more direction to best manipulate the graphene properties to produce any tissue of choice.

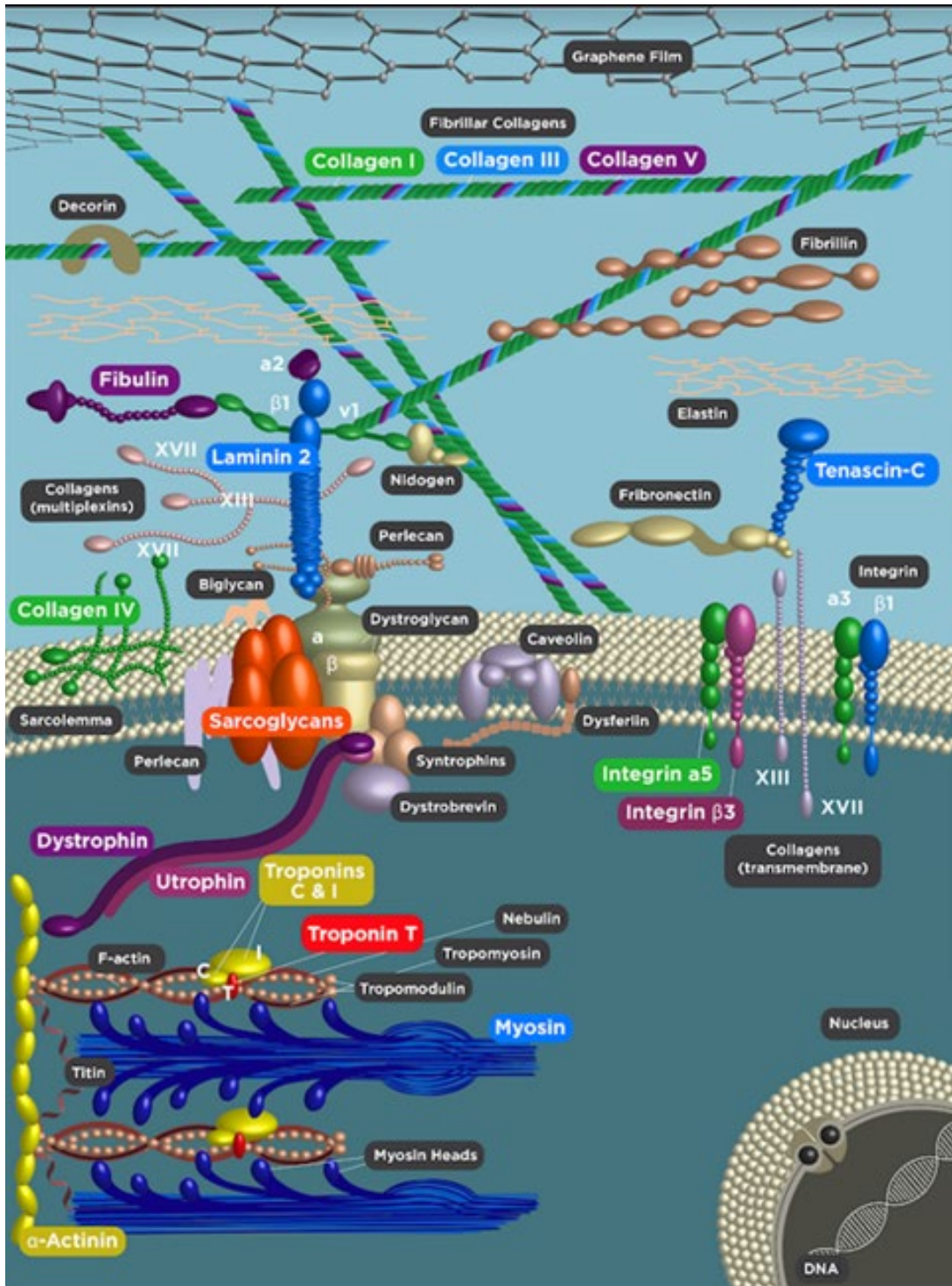


Figure 1.1 Graphene-cell interactions

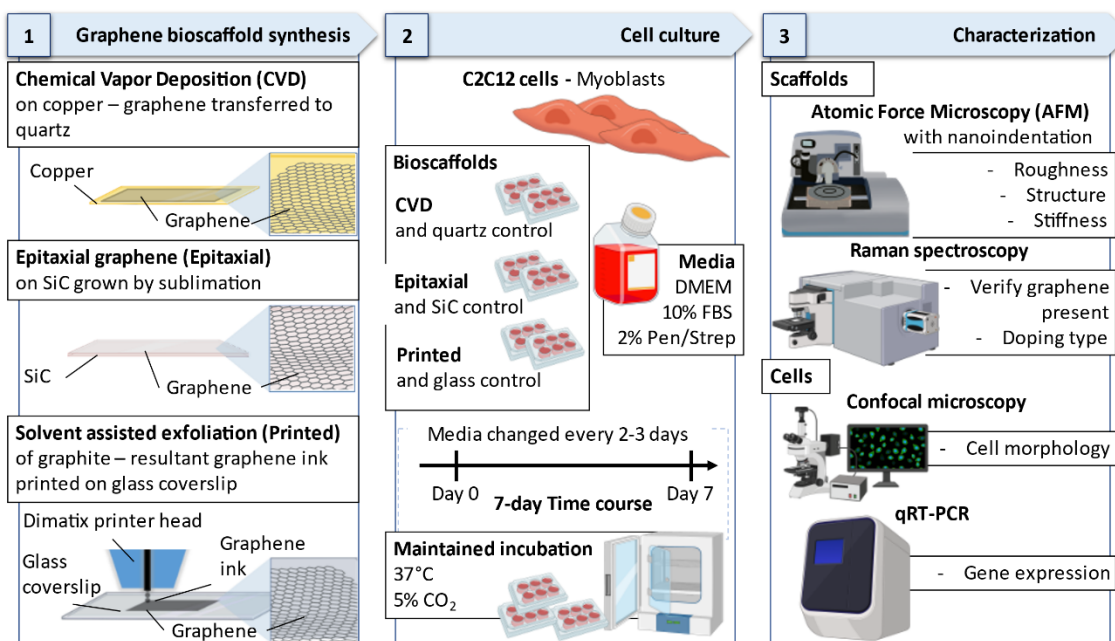


Figure 1.2 Brief outline of experimental methods highlighting, 1) graphene bioscaffold synthesis methods, 2) cell culture methods, and 3) characterization methods performed for cells on the bioscaffolds

CHAPTER TWO: BACKGROUND

2.1 Graphene

Graphene – a crystalline form of carbon is one atom thick and is arranged in a honeycomb-like lattice structure.^{16, 17} The single-layer of sp^2 -hybridized carbon atoms are tightly packed to form a two-dimensional (2D) hexagonal lattice where for every one carbon atom there exists three σ -bonds and a π -bond which exists out-of-plane that allows the carbon atom to bind to neighboring carbon atoms.¹⁸⁻²³ Combined with its atomic structure, graphene consists of many unique properties including high electron mobility at room temperature ($250,000 \text{ cm}^2/\text{Vs}$)²⁴, thermal conductivity ($50000 \text{ W m}^{-1} \text{ K}^{-1}$)²⁵, and superior mechanical properties (Young's Modulus: 1 TPa).²⁶ Its large surface area and extreme chemical stability are also among the properties which make graphene excel in technical areas which produce flexible electronics, supercapacitors, batteries, printable inks, optical and electrochemical sensors, and energy storage.²¹ Graphene was discovered in 2004 by Andre Geim and Konstantin Novoselov who isolated graphene by a physical exfoliation method commonly known as the “Scotch-tape” method.²⁷ The Scotch-tape method obtained graphene by using adhesive tape to peel graphite.¹⁶ Since its discovery, graphene is produced several different ways. To name a few, chemical vapor deposition (CVD), liquid-phase exfoliation (LPE), and epitaxial growth. Graphene can also be derived in various forms some of which are seen in Figure 2.1. In figure 2.1a, graphene's single layer of carbon atoms is seen arranged in their hexagonal honeycomb structure alongside the few-layer-graphene (FLG) seen in figure 2.1b where there are five

layers of graphene stacked on top of each other. Few-layer graphene exists when there is no more than five electrically stacked upon one another.²⁸ When the number of stacked layers exceed five but are below ten layers, this is known as multilayer graphene.²⁸ Ten or more sheets of graphene stacked on one another is bulk graphite²⁸ and is seen in figure 1c. Graphene layer numbers in terms of the superior mechanical, electrical and thermal properties, decrease as graphene layer numbers increases.²⁸ Other graphene derivatives, reduced graphene oxide (rGO) and graphene oxide (GO), are seen in figure 2.1 d and e (respectively). GO and rGO (which is derived from GO) are oxidized versions of graphene which also decrease graphene's mechanical, electrical and thermal properties with the existence of oxides.²⁹ Graphene and its derivatives have been utilized as a cell culture bioscaffold and has cultured various musculoskeletal cell lineages.^{8, 30, 31}

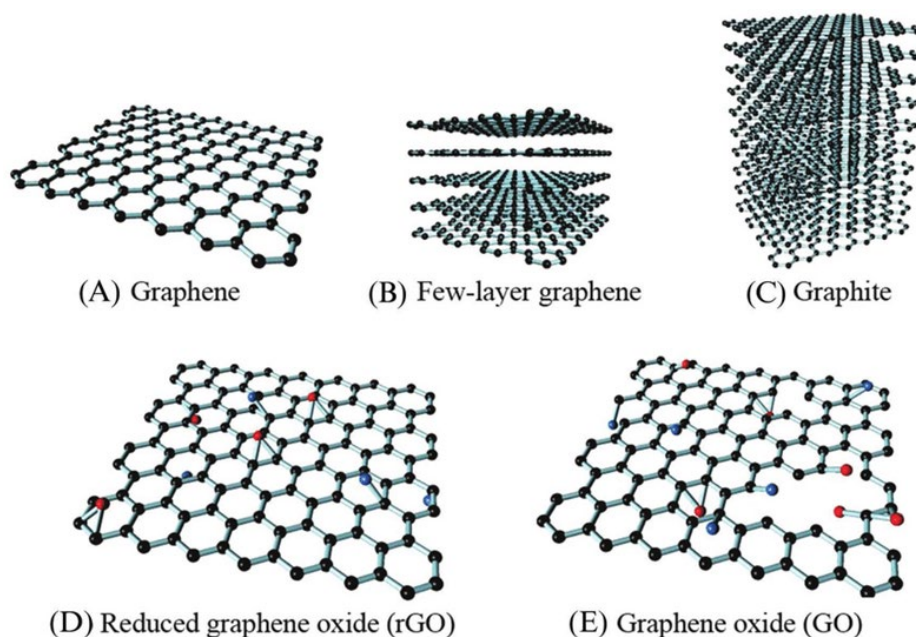


Figure 2.1 Structure of graphene and graphene derivatives a) monolayer graphene, b) few-layer graphene, c) graphite, d) reduced graphene oxide (rGO), and e) graphene oxide (GO)

2.2 Graphene Synthesis

There are various synthesis methods available to obtain graphene and can be categorized by physical or chemical procedures performed. Graphene synthesis techniques include micromechanical exfoliation, also known as the Scotch tape method, epitaxial growth on SiC, chemical vapor deposition (CVD), unzipping carbon nanotubes, liquid phase exfoliation (LPE) of graphite³², and Laser induced graphene (LIG).

Micromechanical exfoliation seen in Figure 2.2 a, utilizes sticky tape (scotch tape), and consists of a series of repetitive graphite peeling.^{33,34} The weak van der Waals interplanar interactions allow isolation of single layers of graphene which can be transferred onto another substrate.^{33,34} Although the highest quality of graphene can be achieved, this method is unsuitable for large-scale production and application. This method is the first method used to obtain graphene by Nobel Prize winners Andre Geim and Konstantin Novoselov in 2010.^{12,33}

The LPE process of graphite— useful in obtaining high concentrations of graphene — is performed to separate graphite layers, held together by van der Waals forces, into individual graphene layers³³⁻³⁵ (Fig. 2.2 b). The LPE phase production process can be divided into three steps: 1) dispersing graphite in a solvent, 2) exfoliation, and 3) purification where exfoliated and unexfoliated flakes are separated by ultracentrifugation.³³⁻³⁵

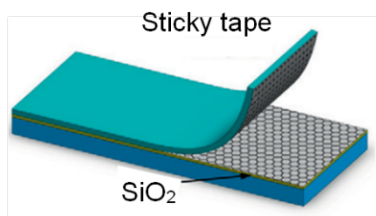
Epitaxial graphene growth (Fig. 2.2 c) processed results in carbon atoms self-assembling on the surface of SiC in a honeycomb lattice structure.^{33,34} Sublimation is the growth mechanism carried out for this type of graphene.³⁴ The process takes place within an ultra-high vacuum (UHV), at temperatures over 1000°C where graphene films are

grown by thermal decomposition of SiC.³⁴ Growing graphene on an electrically insulating substrate such as SiC makes it ideal for high temperature and frequency devices.^{33, 34}

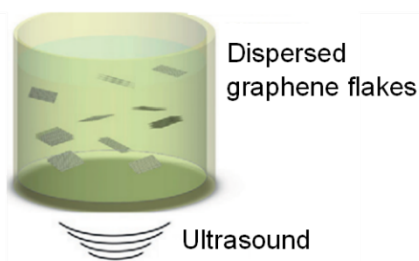
CVD is widely used to manufacture graphene on a large scale and with a high quality^{33, 34} (Fig. 2.2 d). In this process, carbon atoms deposit and nucleate on a substrate. Cu, Ni, and Ni foam are examples of substrates used in the CVD graphene growth process. Graphene grown for experiments in this thesis use Cu as a substrate.

LIG – a multifunctional graphene foam – is made using an infrared laser to scribe on a carbon-based precursor substrate.³⁶ The laser can be pulsed to create an LIG pattern which could be utilized for flexible electronics³⁶.

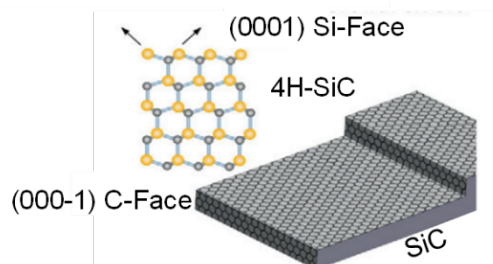
a) Micromechanical exfoliation



b) Liquid Phase Exfoliation



c) Epitaxial graphene



d) Chemical Vapor Deposition

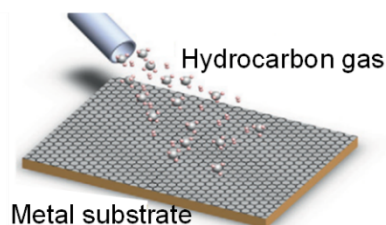


Figure 2.2 Graphene synthesis methods, a) micromechanical exfoliation, b) liquid phase exfoliation, c) epitaxial graphene on SiC, and d) chemical vapor deposition³⁴

2.3 Graphene characterization Atomic force microscopy (AFM) and Nanoindentation

An atomic force microscope is a high-resolution microscope which can acquire atomic level surface images and can determine nanoscale surface roughness, and measure nanoscale mechanical properties of materials.^{37,38} The fundamental principle entails probing a flexible cantilever with a sharp tip back and forth along the surface of a sample. The tip is maintained at a constant force and height as surface measurements are taken. This process is made possible using a feedback mechanism which enables a piezoelectric actuator. In operation of this process, a laser beam, focused on the cantilever, reflects into a photodiode. Throughout the duration of the scan, as the cantilever bends, a photodetector measures the deflection of the laser beam. AFM operation modes include non-contact and contact modes which work by attractive force and repulsive force, respectively. In the last mode, tapping mode, the cantilever lightly taps on the sample's surfaces while oscillating at its resonant frequency.

AFM cantilever-based nanoindentation, a form of instrumented nanoindentation, can determine mechanical properties (Young's modulus) for materials such as thin films³⁸. Fundamentally, displacement of the AFM probe as it contacts the material surface is actuated by a piezoelectric element. The flexible cantilever, upon reaching the material surface, bends from resistive forces from the contact made. Similarly to how the photodetector in AFM measures deflection, a laser beam reflected off the cantilever into the photodiode is monitored. The measured cantilever deflection is converted into force applied to the material with the given knowledge of the cantilever stiffness and the deflection sensitivity. Moreover, the material's indentation depth can be found by a difference between the z-piezo movement and the cantilever deflection.

Surface roughness measurements in this work were performed by a Bruker Dimension FastScan AFM in PeakForce tapping mode. ScanAsyst-Air- HR probe was used to map the topography of the sample surfaces. A Bruker Dimension FastScan AFM with a diamond tip PD nsp probe was used to determine the stiffness of each sample.

Raman spectroscopy

Raman spectroscopy is used to study rotational and vibrational modes in molecules and materials by measuring the inelastic scattering generated by light interactions which occur with the molecule or material. The data acquired through this technique comes in the form of spectral peaks for which each spectral peak is derived from a molecular or lattice vibration which gives us information about the molecular structure, crystallinity, and residual stress.

In typical Raman spectrum of graphene, the two main characteristic peaks are associated with the phonon vibrational modes. The G-band seen $\sim 1580\text{ cm}^{-1}$, originates from a first order Raman scattering process and the 2D-band seen $\sim 2700\text{ cm}^{-1}$, is a result of the double resonance electron-phonon inelastic scattering process.³⁹ There also exists a peak which corresponds to any existing disorders within the samples, this is known as the D-band.³⁹

D-band is related to crystallite size effect and structural defects in the sp^2 – carbon.⁴⁰ The g-band represents the in-plane vibrational E_{2g} mode of the hybridized sp^2 -carbon.⁴⁰ Defect related peaks are features attributed to the stacking of the graphene sheets and the high edge density.⁴⁰

2D peak position and shape can give an indication of the number of graphene layers. For monolayer graphene, a $< 30\text{ cm}^{-1}$ full width half maximum (FWHM) is the

norm.⁴¹ The 2D peak, for bilayer and trilayer graphene, becomes broader and does require multiple Lorentzian fits.⁴¹ The 2D-band energy increases significantly with the increasing layer number.⁴² For monolayer graphene, the 2D peak is seen to be double the height or intensity of the G peak. Previous studies show a good correlation with the number of graphene layers and the 2D to G band intensity ratio⁴², however, considering the ratio alone could not be enough because it is also a benchmark for graphene doping.⁴³

A cause in shift of the G- and 2D- bands is often due to strain or doping of a combination of both.^{43,44} With respect to pure undoped graphene, p-type doping is seen when the 2D peak energy blue-shifts and n-type doping is seen when the peak red-shifts. In p- and n-type doping, the G-band shifts to higher wave numbers.^{43,45}

In this work a Horiba LabRAM HR Evolution Raman microscope was used to collect raman spectral maps over a 10 μm x 10 μm area for each sample. Labspec6 was used to analyze the data acquired.

2.4 Graphene-based bioscaffolds

Graphene's versatility throughout different technological fields has also proven versatile in the biological and tissue engineering field. Graphene's properties have been useful for a wide range of applications in the biological and biotechnology fields which include drug delivery systems, neural interfaces, modulating cell interfaces, and cell scaffolds.

Graphene-based substrates with direct relation to tissue engineering that are currently in literature: graphene film, graphene foam (GF), epitaxial graphene, and previously mentioned graphene derivatives, graphene oxide (GO) and reduced graphene

oxide (rGO). The utilization of these different graphene forms have proven success for a variety of tissue types.

Osteogenic differentiation of MSCs were observed by Xie et al., where it was found that graphene's elastic and surface features alone were what influenced cell differentiation.¹¹ Graphene's topographical effect has been studied by introducing graphene scaffold patterning to influence cell alignment.^{10, 13} Bajaj et al. demonstrated C2C12 myogenic differentiation on graphene patterns fabricated by photolithography. Table 2.1 highlights studies in which graphene has been utilized as bioscaffold for musculoskeletal tissue.

Table 2.1 Graphene bioscaffolds used in musculoskeletal tissue engineering

Tissue	Synthesis method	Bioscaffold	Cell line	Gene Expression Analysis		Ref
				(No (N), Yes(Y), Intracellular (I), Extracellular (E))		
Muscle	Solution cast GO thermally reduced to graphene	Ultra-thin thermal reduced graphene film on glass	C2C12	Y I & E		46
	CVD on Cu	Graphene/SiO2/Si	C2C12	N		13
	CVD on Cu	Crumpled Graphene/PDMS/ VHB	C2C12	N		10, 30,
	CVD on Cu	Graphene film on SiO2/Si & Graphene oxide film on SiO2/Si	SAOS-2	Y I & E		47
Bone	CVD on Cu	Graphene film/ SiO2/Si	hMSCs	Y I & E		31
	CVD on Cu	Graphene film/ PDMS	hBMMSCs	Y I & E		48
	CVD on Cu	Graphene film on: glass, SiO2/Si and stainless steel	OB-6	Y I & E		49
	CVD on Cu	Graphene film/ glass	hPSCs	Y I & E		12
	CVD on Cu	Graphene Nanogrids/PDMS/ SiO2	hMSCs	Y I & E		50
	Radio frequency (RF)/plasma CVD	CNWs (Carbon nanowalls) on Thermanox	SAOS-2	Y E		40
	CVD on Cu	Graphene film/Ti	hMSCs	Y I & E		22
	CVD on Ni	Graphene film/ PDMS	hDPSCs	Y I & E		11
Bone-ligament	CVD on Cu	Graphene film/ glass	hPDLSCs	Y I & E		51

2.5 The Musculoskeletal System

The musculoskeletal system grants the body stability and form, enables the body to move, and protects the internal organs.⁵² This system, comprised of bones, muscles, tendons, ligaments, joints, cartilage, and other connective tissues, is seen in Figure 2.3

Bones are calcium rich and are what make up the body's skeleton which consists of 206 bones.^{53, 54} Trabecular (spongy) and cortical (compact) bone are the two basic types of bone which differ in microarchitecture and porosity.⁵⁴ Compact bone is surrounded by a thin membrane of tissue known as the periosteum which is made up of connective tissue, blood vessels and nerves.⁵⁴ Although not all bones contain bone marrow, for those which do, the bone marrow is located within trabecular bone.⁵⁴ Specialized cells which include stem cells, are found within the bone marrow.⁵⁴ These specialized cells produce blood cells.⁵⁴

The skeletal model displaying the skeletal bone (left) and skeletal muscle (right) in Figure 2.3 a highlights the main joints found through the human body. The joints – a junction where two or more bones meet – are visible on the left side of the skeletal model, give a clear view of articular cartilage that exists on the ends of the long bones. Articular cartilage provides cushion within joints and alleviates friction during movement which allows bones to glide over one another.²¹ This type of cartilage is found in the various types of joints such as the ball and socket joint seen in the shoulder and the hips, the hinge-joint seen in the elbow, knee and ankle, the pivot joint seen just below the elbow, the saddle joints in the hand, and plane joint seen in the feet. The skeletal muscle (right) in the skeletal model (Fig. 2.3 a) shows how muscle covers each joint.

Figure 2.3 b focuses on the knee joint and highlights some of the other connective tissues that work together in stabilizing the knee. Ligaments are tough bands of mainly collagen and elastin fibers and are what bring two or more bones together by connecting from bone to bone to form a joint (Fig. 2.3 b). The stability of a joint is strongly dependent on the presence of ligaments.

Tendons are responsible for joint movement and create the muscle to bone connections and can be seen in Figure 2.3 b. When muscles contract, the contraction of the muscles is transferred to bones through the tendons.

Skeletal muscles, one of three types of muscle found in the body, are categorized as voluntary muscles and enables control over body movement. The remaining two muscle types, cardiac and smooth muscle, are categorized as involuntary muscle; functioning without having to put thought into the action. Examples of involuntary muscles at work include the heart (cardiac muscle) beating and the kidneys (smooth muscle) working to remove waste from the body. Connective tissue, blood vessels, and nerves are contained in skeletal muscle. The three layers of connective tissue are called the epimysium, perimysium, and endomysium.

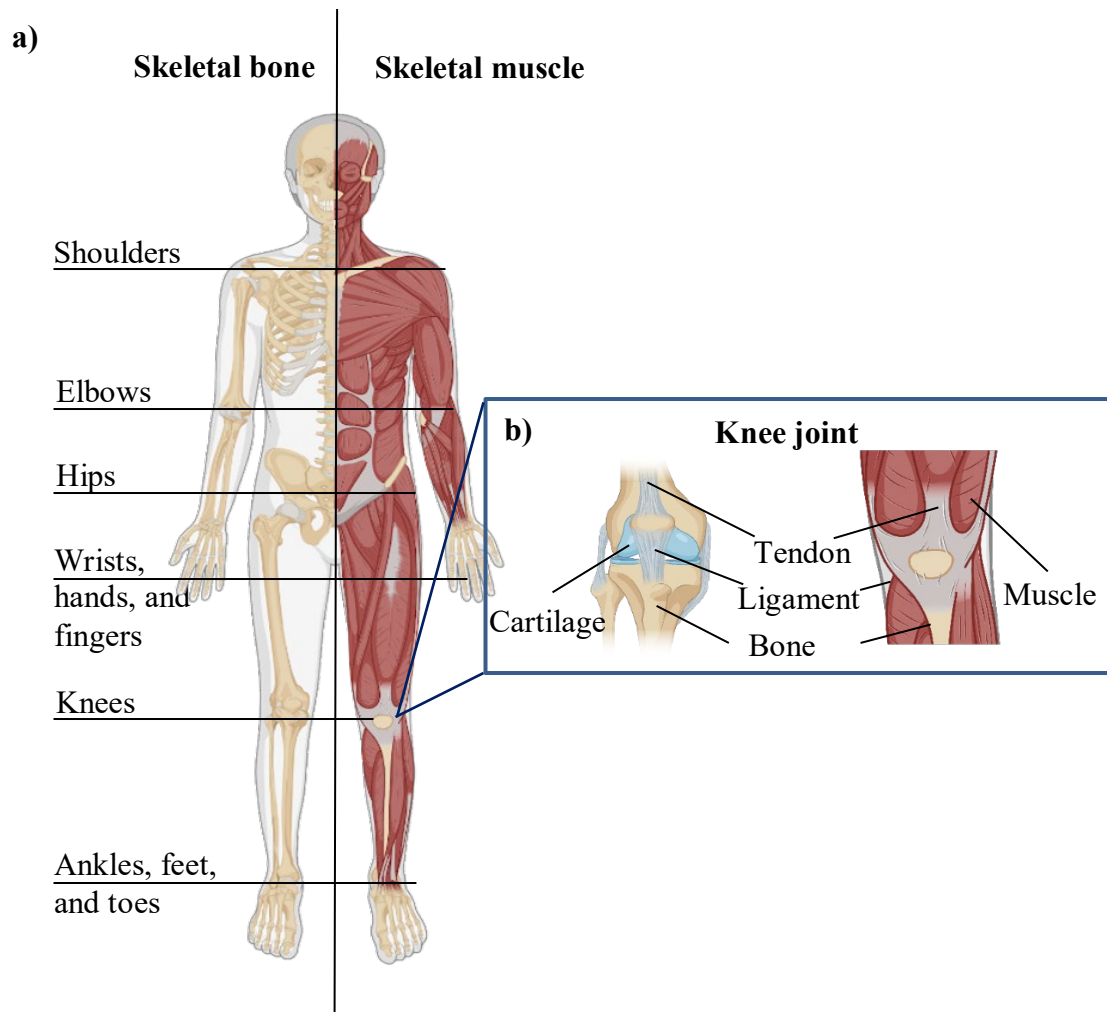


Figure 2.3 The musculoskeletal system can be split into two parts, a) skeletal bone (left) and skeletal muscle (right). Joints (labeled by body part) are formed by bones, cartilage, ligaments, muscle, and other connective tissues and is seen in b) which represents a close up of the knee joint. (Figure by Biorender)

2.6 Skeletal muscle composition, structure and function

Skeletal muscle as it attaches to skeletal bone by a tendon is seen represented in Figure 2.4. Mature skeletal muscle tissue is composed of muscle fibers bundled together by connective tissue sheaths.⁵⁵ The outer most sheath is known as the epimysium, and it contains bundles of fasciculi, which are covered by a connective tissue sheath called the perimysium.⁵⁵ Every fascicle contains a bundle of muscle fibers which are enclosed by

the endomysium, the innermost connective tissue.⁵⁵ Numerous myofibrils containing myofilaments are contained within each muscle fiber.⁵⁵ Myofibers are elongated multinucleated fibers that form when myoblasts fuse.² Sarcomeres are fundamental elements in muscle contraction⁵⁵ and are what give muscle their striated appearance.

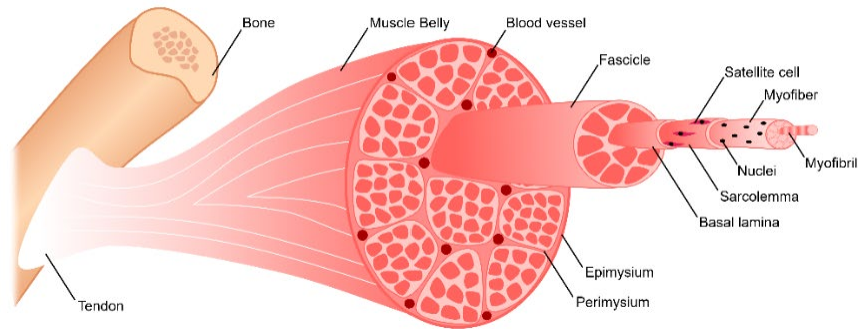


Figure 2.4 Components of skeletal muscle as it attaches to bone through the tendon²

Myogenesis is a complex process which takes place when muscle is being formed. Precursor cell migration, myoblast proliferation, cell cycle arrest, and terminal differentiation of myoblasts are events which take place during myogenesis.¹ Other events include muscle-specific gene transcription and myoblast fusion.¹

The extracellular matrix (ECM) is a crucial component in the myogenesis process and for muscle function.⁵⁶ The ECM is composed of three main proteins; collagen, non-collagen, and proteoglycans.⁵⁷ The matrix also contains receptors and regulators such as integrin and matrix metalloproteinase (MMP).⁵⁷ The ECM facilitates cell-matrix interactions required for physiological muscle activity⁵⁷ by providing a microenvironment which is stable and supports functions such as, adhesion, migration, proliferation and differentiation.⁵⁷

The most abundant protein found in the body is collagen, and it is what makes up most of the ECM in the bodies connective tissues such as skin and tendons as it provides tensile strength.^{57, 58} Collagen exists in several subtypes namely, Type I, III, V, and XI, and form collagen fiber found in skeletal muscle.⁵⁷ Collagen also plays a role in cell adhesion and migration.⁵⁸ Elastin, also a structural protein, works simultaneously with collagen as it provides tissues like tendons the ability to recover after being stretched continuously.⁵⁸

Fibronectin, plays a key role in cell adhesion, and wound healing response in tissue injury.⁵⁸ The protein forms a fibril mesh and is connected to cell surface receptors like integrins.⁵⁸ It promotes myoblast adhesion, and differentiation where it helps with alignment and myotube fusion.⁵⁷ Similar to fibronectin, laminins are involve in cell differentiation and adhesion.⁵⁷ They also promote the activation and expression of integrins.⁵⁷

Dystrophin and dystroglycan link the cytoskeleton to the ECM and are important for maintaining the integrity of the membrane.⁵⁷ These proteins with the help of others such as dystrobrevin and utrophin form the dystrophin-glycoprotein complex (DGC)⁵⁷ and attaches to the ECM through laminin.⁵⁷ Proteoglycans (PGs) are important in skeletal muscle as it connects the internal components of the cytoskeleton to the ECM.⁵⁷

2.7 C2C12 cells

C2C12 cells are an adherent, biopotential murine cell line⁵⁹ and is a widely used cell culture model for skeletal muscle studies.⁶⁰ These cells are known for their ability to rapidly differentiate and form contractile myotubes.⁶¹

The typical morphology seen for myoblasts are structures with more elongation⁶⁰,⁶² as opposed to that of the cuboidal structures seen for osteoblasts.⁵⁹ When growth media is supplemented with bone morphogenic protein 2 (BMP-2), C2C12 cells are seen to shift differentiation pathways from myoblastic to osteoblastic.⁵⁹

Myogenic regulatory factors (MRFs) which regulate the differentiation of C2C12 cells are myogenic factor 5 (Myf5), myogenic differentiation antigen (MyoD), myogenin (MYOG), and myogenic factor 4 (MRF4).⁶³ Myosin heavy chains (MHCs) play a role in skeletal muscle function, growth and development of skeletal muscle.⁶³

CHAPTER THREE: MANUSCRIPT

3.1 Abstract

Graphene – an atomically thin layer of carbon atoms arranged in a hexagonal lattice – has gained interest as a bioscaffold for tissue engineering for its exceptional mechanical, electrical, and thermal properties. Graphene’s structure and properties– tightly coupled to synthesis and processing conditions– yet their influence on biomolecular interactions at the graphene-cell interfaces remains unclear. In this study, C2C12 cells were grown on graphene bioscaffolds with specific structure–property– processing–performance (SP3) correlations. Bioscaffolds were prepared by chemical vapor deposition (CVD), sublimation of Silicon Carbide (SiC), and printed solvent assisted exfoliated graphene ink. To investigate the biocompatibility of each scaffold, cellular morphology and gene expression patterns were investigated using the bipotential mouse C2C12 cell line. Using a combination of fluorescence microscopy and qPCR we demonstrate that graphene production methods determine the structural and mechanical properties of the resulting bioscaffold, which in turn determine cell morphology, gene expression patterns and cell differentiation fate. Therefore, production methods for graphene bioscaffolds must be chosen carefully when considering graphene as a bioscaffold for musculoskeletal tissue engineering.

3.2 Introduction

Musculoskeletal conditions are often debilitating and can cost the US an estimated \$213 billion in lost wages and treatments that are generally limited to symptomatic relief from invasive surgery or total replacement.⁶⁴ Volumetric muscle loss can be especially challenging to treat due, in part, to the absence of the extracellular matrix (ECM) which removes the biophysical and biochemical signaling cues that aid in regeneration.⁶⁵ One potential solution for treating these injuries is through the transplantation of muscles to replace damaged tissue. While this has had some measure of success, this approach requires a suitable muscle tissue donor or donor site which is limited and creates additional injury.⁵ Promising alternatives to transplantation for skeletal muscle regeneration include physical therapy, cell therapy, nanotechnology, and tissue engineering.⁶⁶ While these options may overcome many of the associated challenges, advances are needed to make tissue engineering a viable solution.

Tissue engineering approaches involve the utilization of biocompatible scaffolds to support cell growth and attempt to replicate biophysical properties found in the native tissue. Bioscaffolds should provide structural support, facilitate cell adhesion, deliver molecular signals such as growth factors, and replicate or induce cells to produce ECM that matches the native tissue microenvironment.⁶⁵ Tissue engineered bioscaffolds serve as a template for tissue formation and can be seeded with stem cells and growth factors to augment the healing process.⁶⁷ While there have been tremendous advances in tissue engineering approaches, more research is needed to develop suitable biocompatible scaffolds. In this regard, graphene has emerged as a viable bioscaffold for many tissue engineering applications.

Graphene bioscaffolds are utilized with various cell types, such as cardiomyocytes,²⁰ neuronal cells,^{14, 15} mesenchymal stem cells,⁶⁸ and myoblasts⁶⁹ to generate numerous different tissue. Graphene bioscaffolds have many promising attributes including biocompatibility, serum protein absorption, high tensile strength, and electrical conductivity. Graphene has even shown to promote differentiation of certain musculoskeletal cell lines.⁶⁹⁻⁷²

Since the realization of graphene in 2004, numerous methods to produce graphene have been developed including micromechanical exfoliation, laser induced graphene, chemical vapor deposition (CVD), liquid phase exfoliation (LPE) of bulk graphite, and epitaxial growth.^{35, 73} Each of these methods have benefits and limitations such as graphene quality, grain sizes, yield, and the number of layers. True monolayer graphene consists of a single layer of carbon atoms arranged in a hexagonal honeycomb structure. Bilayer or few-layer-graphene are often used in bioscaffold studies; however, the number of graphene layers alters the mechanical, electrical, and thermal properties of the material.²⁸

Researchers have explored various geometries of graphene such as patterned islands,¹³ crumpled bioscaffolds,¹⁸ and CVD hybrids.¹⁹ Bajaj et al. found that C2C12 cell growth aligned with the graphene patterned islands.¹³ Kim et al. found that their crumpled graphene promoted alignment, elongation, differentiation, and maturation of the C2C12 cells.¹⁸ Although numerous studies have evaluated graphene bioscaffolds, very few studies focus on the impact of different graphene synthesis methods on a cell line, making it difficult to correlate the relationship between graphene analogs and cellular dynamics.

Here we report on our evaluations of the structure-properties-processing-performance relationship of graphene bioscaffolds produced using three synthesis methods and the effects each has on the growth and differentiation of murine C2C12 cell towards myogenesis. A schematic representation of graphene synthesis and experiment outline is shown in Figure 3.1.

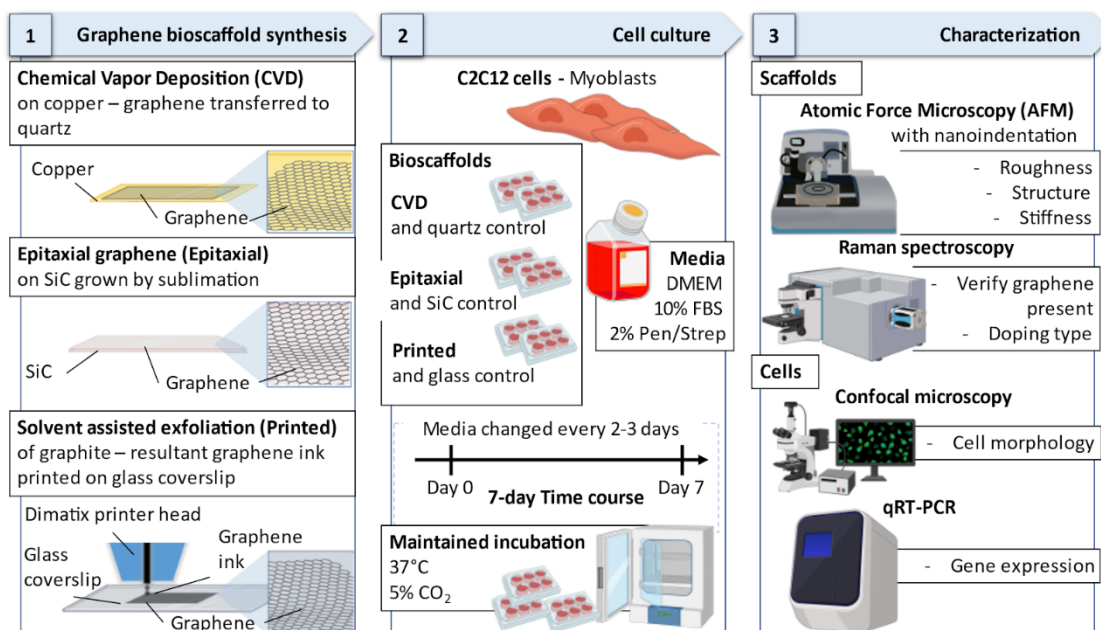


Figure 3.1 Schematic of the different graphene synthesis methods, cell culture outline, and the characterization techniques utilized.

Graphene bioscaffolds were produced by CVD, LPE, and sublimation of Silicon Carbide (SiC). Each scaffold has various physicochemical properties leading to changes in cellular dynamics and morphologies. Our cell-based studies also reveal distinct genetic profiles of C2C12 cells grown on each graphene bioscaffold. Collectively, we demonstrate that synthesis methods for the construction of different planar graphene bioscaffolds impact the material's properties and ultimately cell growth dynamics.

3.3 Results

Graphene Characterization

To investigate how variations in graphene's structure and properties affect cellular growth dynamics, we used three common methods to produce graphene; graphene grown by CVD on copper foil, epitaxial growth via sublimation on SiC, and LPE. After obtaining the graphene, the samples were deposited onto different substrates. For graphene grown by CVD, the graphene film was removed from the Cu foil by electrochemical delamination and transferred to quartz. An ink was formulated out of the LPE graphene and deposited on a glass coverslip using inkjet printing. Graphene grown via thermal decomposition of SiC was utilized as prepared.

Atomic Force Microscopy (AFM) and Raman spectroscopy were performed to characterize graphene bioscaffolds and identify the varying properties that may impact downstream cellular dynamics. Specifically, AFM was utilized to determine the surface characteristics and stiffness of each bioscaffold (Figure 3.2). Topography measurements were collected across a random 10 μm x 10 μm area of each scaffold and used to calculate the average surface roughness. CVD graphene (Figure 3.2a) had the most uniform surface, with peaks reaching up to 10 nm and had an associated Ra of 1.29 nm. SiC graphene (Figure 3.2b) revealed a layered structure along the surface, with peaks up to 12 nm and a RA of 1.74 nm. The printed graphene (Figure 3.2c), as expected, had the roughest surface, with peak to valley measurements reaching up to 160 nm and displayed a surface roughness of 15.0 nm.

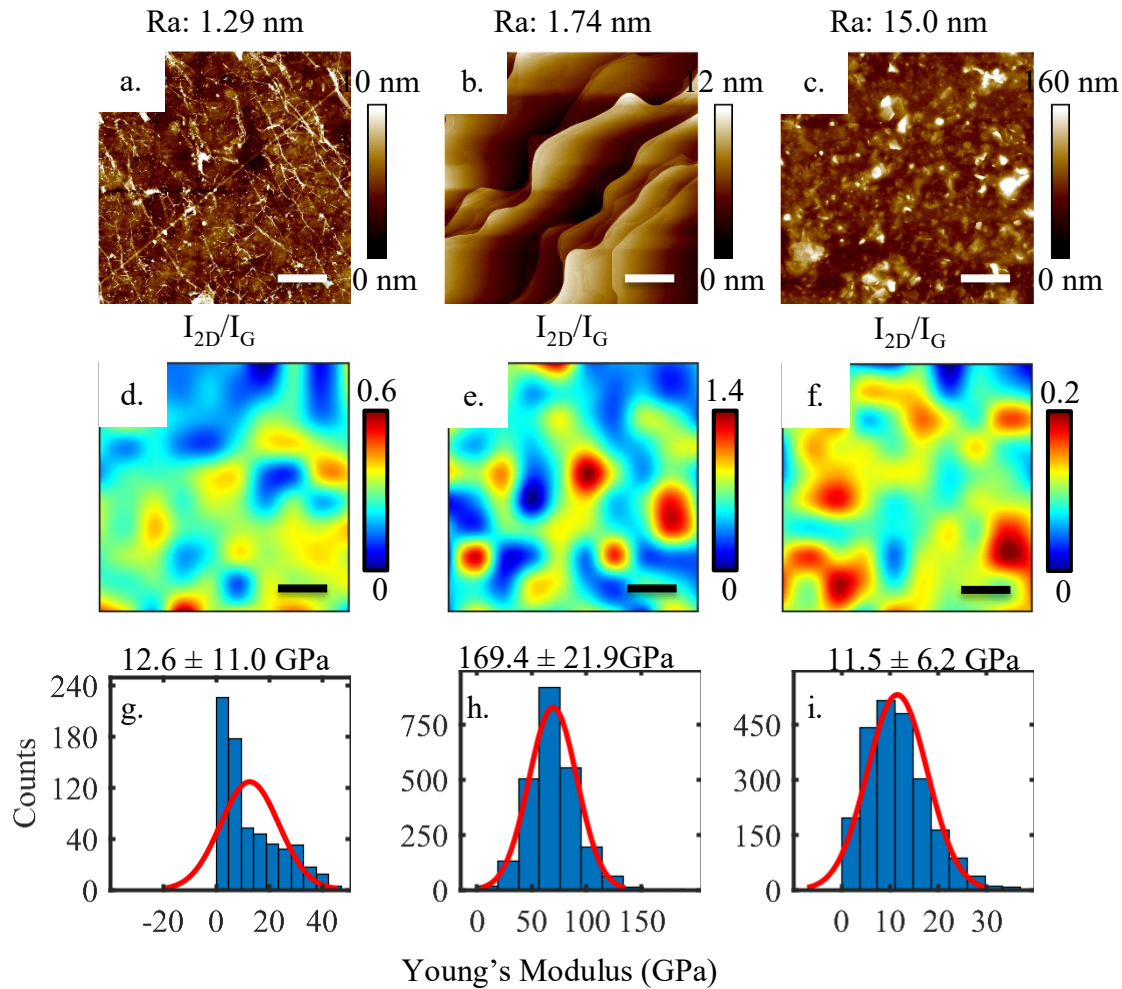


Figure 3.2 Graphene bioscaffold characterized by AFM, Raman spectroscopy, and Nanoindentation. Structure and roughness taken by AFM for a) CVD, b) Epitaxial, and c) Printed. Raman intensity maps for 2D- and G- peak ratios for d) CVD, e) Epitaxial, and f) Printed. Nanoindentation histograms representing bioscaffold stiffness for g) CVD, h) Epitaxial, and Printed. (AFM and Raman map scale bar = $2\mu\text{m}$)

The Raman spectra of graphene has three characteristic peaks near 1580, 1350 and 2700 cm^{-1} known as the G, D, and 2D peaks, respectively. The ratio of the intensities of the 2D to G peaks is related to the number of layers in graphene which can have significant impacts on its properties.⁷⁴ Raman spectroscopy maps of the 2D (I_{2D}) to G (I_G) peak intensity ratios (I_{2D}/I_G), are shown in Fig. 3.2d-f. The printed graphene sample had

the largest surface features along with the lowest 2D to G peak ratio (0 to 0.2) indicating multilayered structures throughout the sample. The epitaxial graphene bioscaffold showed the highest I_{2D}/I_G ratios ranging from 0 to 1.4, indicating more monolayer to few layers graphene present when compared to the other graphene samples.⁷⁴ Even though the CVD graphene had the smallest surface roughness, the Raman map ratios indicate more layers than epitaxial grown graphene but have a more uniform formation.

The Young's modulus (GPa) for each bioscaffold is shown in Fig. 3.2h-j. Stiffness measurements were obtained by nanoindentation using an AFM.⁷⁵ Epitaxial graphene (Fig. 3.2h) showed the highest average stiffness (69.4 GPa), followed by CVD graphene (12.6 GPa; Fig. 3.2j), and printed graphene, which had the lowest value (11.5 GPa) for stiffness (Fig. 3.2i). All values obtained are all considerably lower than their associated substrates and the theoretical Young's modulus of graphene, suggesting that these values are mostly influenced by the graphene scaffold fabrication method.

Cell Growth and Morphology

The mouse muscle precursor C2C12 cell line is a well-documented cell line that is often used to study myoblast proliferation and differentiation which has been invaluable for *in vitro* studies that aim to understand myogenesis.⁷⁶ To evaluate how the three different graphene bioscaffolds impact cellular growth dynamics, C2C12 cells were seeded on the scaffolds and cultured for seven days. Each well containing the graphene scaffold was first coated with agarose gel to promote the cells to only grow on the graphene so that changes in morphology and genetic expression profiles were not impacted by cells growing off the scaffold.

Changes in cell morphology in response to the three graphene bioscaffolds is shown in Figure 3. For controls, cells were also cultured on the three different substrates (quartz, SiC, and glass) that the graphene was deposited onto. After a seven-day culture, the C2C12 cells displayed dramatically different cell morphologies between the three graphene bioscaffolds and the corresponding controls.

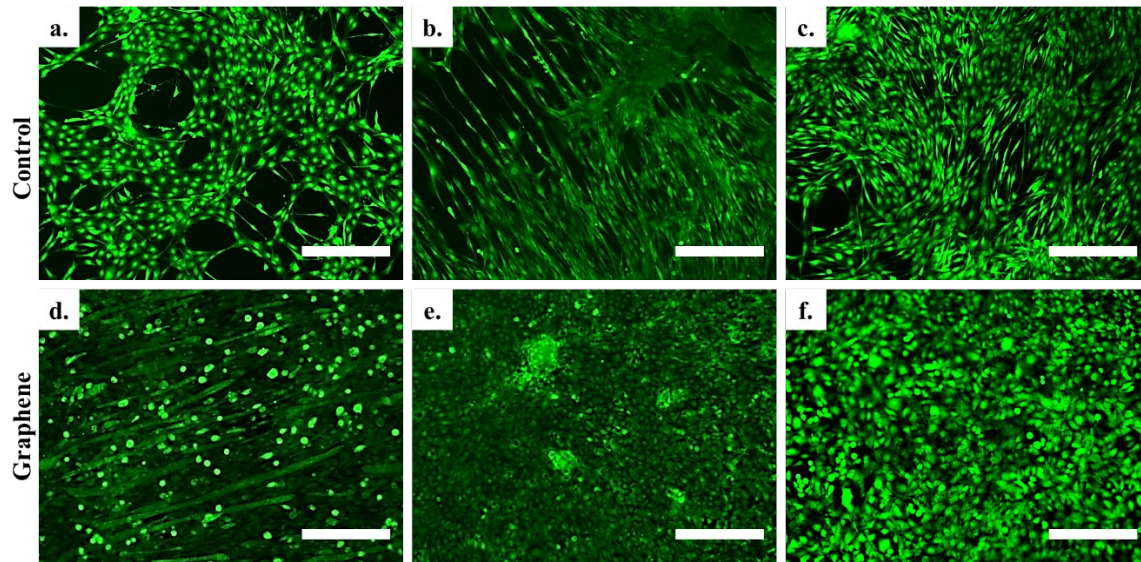


Figure 3.3 Calcein-AM stained C2C12 images taken by optical microscope show cell morphology was influenced by graphene bioscaffolds and control substrates. Control substrates a) Quartz, b) SiC and c) glass coverslip, and graphene bioscaffolds d) CVD, e) Epitaxial and f) Printed. (Scale bar = 300 μm)

The C2C12 cells grown on the control substrates all resulted in different morphologies. The quartz surface (Fig. 3.3a) resulted in a rounded, cobblestone-like morphology, compared to elongated cells present on the SiC (Fig. 3.3b) and glass (Fig. 3.3c) substrates. However, this didn't translate to the cells grown on the graphene scaffolds deposited onto the various substrates. The CVD grown graphene bioscaffold (Fig. 3.3d) resulted in an elongated cell morphology, comparable to what would be expected for myoblasts, but in contrast to the quartz control. Epitaxial graphene bioscaffolds (Fig. 3.3e) and printed graphene bioscaffolds (Fig. 3.3f) resulted in cells that

had a more rounded, cobblestone-like morphology, which again was different from their respective controls. Additionally, epitaxial and printed graphene bioscaffolds supported the formation of tightly packed nodules of cells. No cellular nodules were observed for the cells grown on the printed graphene bioscaffold. The cells grown on the CVD graphene bioscaffold were the only ones to demonstrate an elongated cellular morphology, when compared to the other graphene samples.

Since the cell morphology differences were distinctive and are often indicative of cell differentiation lineages, we quantified the differences in morphology by measuring the aspect ratio and alignment of the cells for the different growth conditions. Figure 3.4 shows the aspect ratios measured for the CVD, epitaxial, and printed graphene bioscaffolds plotted next to their respective control surfaces. Following similar methods as Wang et al., the longest length of the cell structure and the shortest width were measured for 30 cells for each condition.⁷⁷ Aspect ratios for quartz, epitaxial graphene, and printed graphene were all near a value of 1, indicating a spherical shape. The other samples (glass, SiC, and CVD graphene) contained more extended morphologies, all with ratios below 0.2. When comparing the graphene samples, the only one to display a low aspect ratio was the CVD grown bioscaffold.

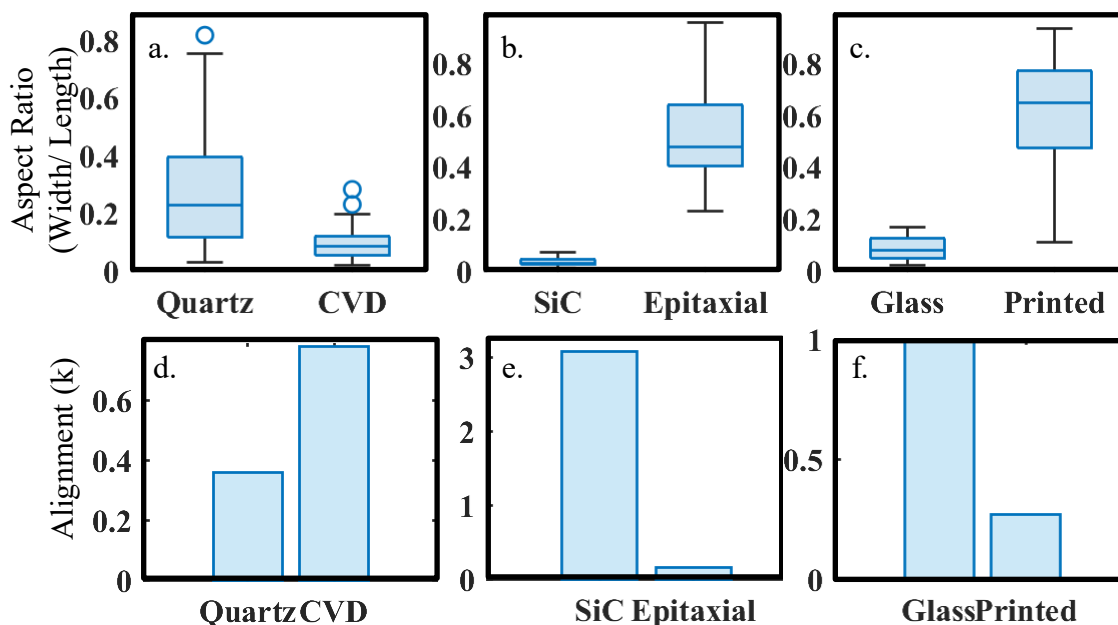


Figure 3.4 Aspect ratio and alignment studies reveal quantitative morphological differences between the graphene bioscaffolds and respective controls. Aspect ratios for a) Quartz is higher than CVD, b) Epitaxial is higher than SiC control, and c) Printed is higher than glass. Alignment analysis show more alignment in d) CVD over quartz, e) SiC over epitaxial, and f) glass over printed.

Assessment of differential gene expression of differential markers

Muscle cells are typically aligned to form a functioning tissue and cellular alignment is an important factor to consider in tissue engineering applications. To compare the alignment values (k), the CVD, epitaxial, and printed graphene were plotted along with their respective control surfaces (Fig. 3.4d-f). A higher degree of alignment is indicated by larger k-values.⁷⁸ Fiber orientation (μ), sigma and R^2 were also calculated (see supporting information S1). All samples showed distinctive differences in their alignment values, with the biggest differences noted between the epitaxial graphene and SiC which had the highest k-value of all the samples measured. Of the three graphene samples, only the CVD graphene had a higher alignment value than its control.

Genetic Expression Profiles

To understand the impact that the graphene scaffold had on the cell's genetic expression profiles, qPCR was performed on the graphene scaffolds and compared against their controls. Thirty-five genes related to ECM and muscle cell differentiation were analyzed. Figure 5a shows differential gene expressions as a heatmap of \log_2 fold change versus their respective controls. The heatmap includes genes encoding proteins that play a role in attachment, myogenesis, ECM, contractility, and matrix remodeling. For each functional group of genes, a radar plot was created to display genetic expression level changes for select genes to compare the differences between the three graphene bioscaffolds (Fig. 3.5b-f).

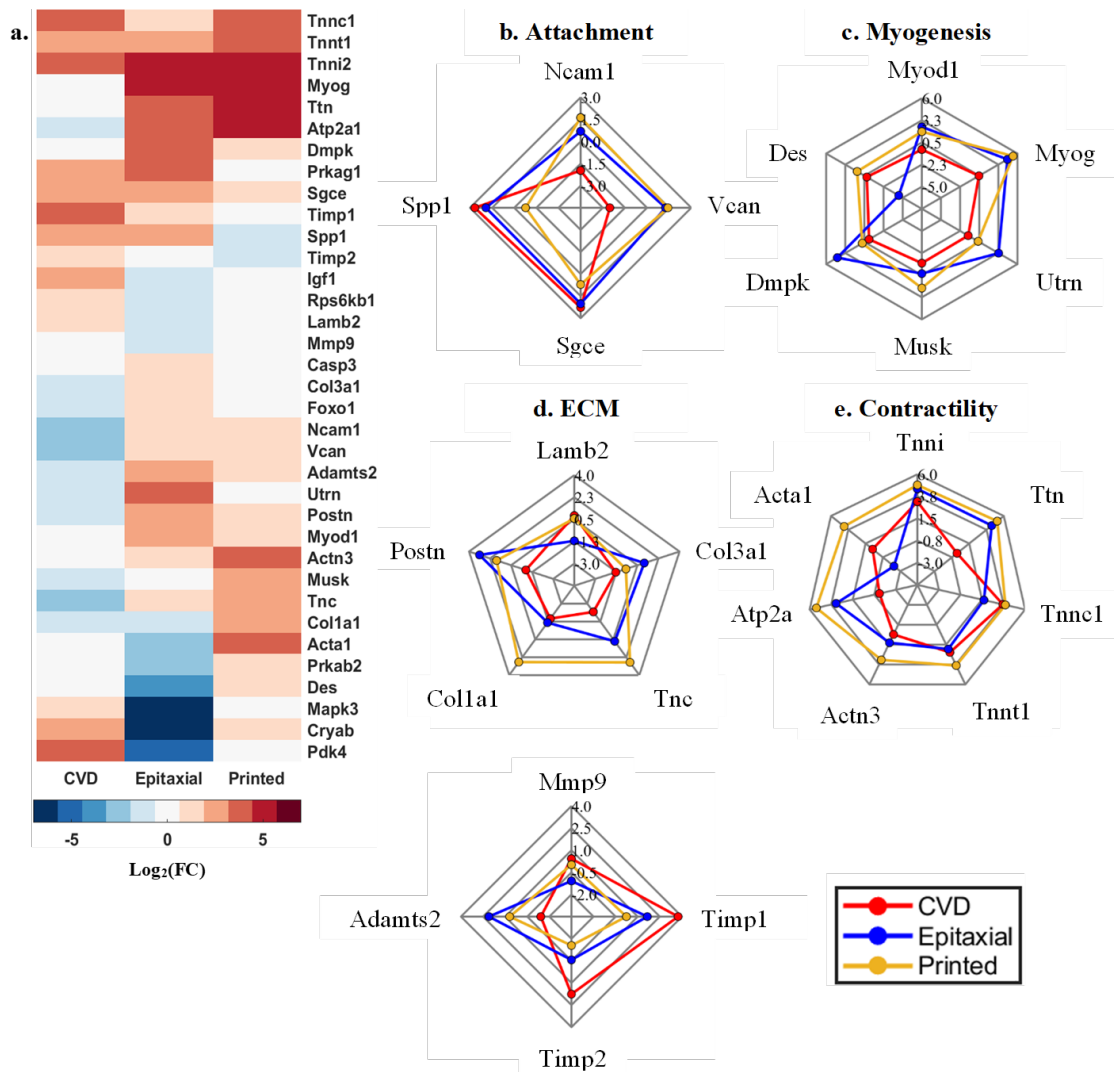


Figure 3.5 a) Heatmap displaying gene expression patterns seen for the three graphene bioscaffolds. b) Genes related to attachment, c) genes related to myogenesis, d) genes related to contractility, e) genes related to ECM, and f) genes related to remodeling. (Tables 3.1, 3.2, 3.3, 3.4 and 3.5 highlight gene functions)

Six genes involved in myogenesis, *Myod1*, *Myog*, *Utrn*, *Musk*, *Dmpk*, and *Des* are highlighted in the radar plot (Figure 3.5c). Each of these genes were upregulated for cells grown on the printed graphene bioscaffold and all but *Des* was upregulated on the epitaxial graphene bioscaffold. Interestingly, even though the morphology of the cells on the CVD graphene appeared the most myotube like of the three graphene samples, the

was only a minor downregulation of a few of the genes with the rest mostly unchanged (*Myod1*, *Utrn*, *Musk*, and *Dmpk*).

Since all three graphene samples had different surface roughness, graphene layer numbers, and stiffness, it is likely that cellular attachment is impacted. Genetic expression levels of genes related to cell attachment are highlighted in Figure 3.5b. All graphene bioscaffolds, induced upregulation of *Sgce* and may be related to cellular attachment to graphene in general, regardless of the varying properties of the material. *Ncam1* was down regulated in cells grown on CVD and printed graphene and *Vcan* was upregulated in cells grown on both epitaxial and printed graphene bioscaffolds. *Spp1* was upregulated in cells grown on CVD and epitaxial graphene but was downregulated on printed graphene. However, all four genes evaluated were upregulated on the epitaxial graphene bioscaffold.

Extra cellular matrix production from cells is an important factor for bioscaffolds aiming to replicate native tissue. To understand the effect of the different scaffolds on ECM production, genes that are involved in ECM production were evaluated. *Lamb2*, *Tnc*, *Colla1*, *Postn* were upregulated on the printed graphene bioscaffold, while *Col3a1* was downregulated. *Col3a1* was upregulated on the epitaxial bioscaffold but downregulated on the CVD grown graphene. *Col3a1* was one of the four out of five genes that was downregulated on the CVD bioscaffold. *Tnc*, *Colla1* and *Postn* were also downregulated on CVD where like the printed graphene, *Lamb2* was upregulated. *Lamb2* was one of two (*Colla1*) downregulated genes on the epitaxial bioscaffold – *Col3a1*, *Tnc*, and *Postn* were upregulated.

Similarly, genes related to matrix remodeling were also highlighted in the radar plots (Figure 3.5f) *Timp1* was the only gene upregulated in all three bioscaffolds. For CVD and printed bioscaffolds, *Timp1* was upregulated as was *Mmp9*. *Timp2* was upregulated on the CVD graphene bioscaffold but downregulated on the printed graphene bioscaffold. *Adamts5* was upregulated on the printed graphene bioscaffold and downregulated on the CVD bioscaffold. Like the printed bioscaffold, *Timp2* and *Adamts5* were downregulated and upregulated respectively on the epitaxial bioscaffold.

The ability of muscle cells to contract is an essential part of generating functional muscle tissue, so seven genes related to contractility were evaluated (*Tnni*, *Ttn*, *Tnnc1*, *Tnnt1*, *Actn3*, *Atp2a1*, and *Acta1*). All these genes were upregulated on the printed graphene bioscaffold, while six out of these seven genes were upregulated on epitaxial graphene (*Acta1* was downregulated). *Acta1* was upregulated on CVD graphene along with four other genes. *Atp2a1* and *Ttn* were downregulated on CVD graphene but upregulated on epitaxial and printed graphene bioscaffolds.

3.4 Discussion

Graphene's use as a bioscaffold for tissue engineering applications has been studied by numerous researchers throughout the field. This versatile material has shown to be biocompatible with a variety of cell lines and has a wide range of unique properties such as electrical conductivity that is not usually present in other polymer-based scaffolds. Interestingly, graphene has even been implicated in inducing differentiation of progenitor cells without traditional growth factors present.⁷²

The three graphene synthesis methods resulted in three contrasting structures and properties. Through AFM, the surface scans reveal topographical differences, stiffness,

and average surface roughness for each bioscaffold. Raman maps also revealed differences in the quality of graphene when evaluating by the number of layers present. The CVD graphene had the smoothest surface and had the lowest distribution differences in the I_{2D}/I_G peak ratios, even though the epitaxial graphene had the largest ratio values. The properties seen in the CVD grown graphene translated to different cellular morphologies than the other two graphene scaffolds. Only the CVD graphene displayed elongated and highly aligned cells, indicating more myotube formation as opposed to the cobblestone-like structures seen in epitaxial and printed graphene. This was further apparent when quantifying the aspect ratio and alignment of the cells. However, when looking at the genetic expression profiles, even though some genes related to myogenesis were upregulated in the CVD graphene, the other graphene scaffolds had more genes related to myogenesis upregulated. This could be due, in part, to the fact that the cells grown on the quartz control had aspect ratios and alignment values that were more similar to the graphene scaffold than the other samples evaluated and thus could impact the fold change comparison.

As ECM and muscle assays were the only gene assays utilized in this study, further investigation is warranted to completely understand the impact that the different properties of various graphene scaffolds have on the differentiation of cells. Additionally, other properties of the graphene such as the electronic nature of the material may influence cell growth dynamics. Analysis of the different graphene scaffolds was performed and revealed that the CVD and printed graphene samples appear to be n-type, whereas the epitaxial grown graphene appeared to be p-type (Supporting Info Figure 3.6, 3.7, and 3.8) but more in-depth investigations are needed to understand how this property

may impact different cells. While there are other properties and target genes that warrant evaluation, this work demonstrates that variations in graphene properties can dramatically impact cell growth dynamics and genetic expression profiles. This highlights the need for researchers to fully characterize and report on the graphene properties so that studies aimed at utilizing graphene as a bioscaffold can be more informed and further advance graphene as a viable scaffold for tissue engineering applications.

3.5 Conclusion

This study demonstrated that graphene production and scaffold fabrication methods result in different structures and characteristic properties which ultimately impact cellular morphology and genetic expression profiles. Graphene layer number, roughness, stiffness, and electronic nature were characterized prior to cell culture. The C2C12 murine precursor muscle cells were cultured on the different scaffolds, and all induced different cell growth dynamics after seven days of culture. All three scaffolds caused different morphologies and genetic expression profiles. The CVD grown graphene appeared to induce more myotube formation but didn't necessarily translate to upregulation of the genes involved in myogenesis that were evaluated. Understanding how different properties of various graphene analogs impact differentiation and growth dynamic could prove useful when attempting to produce a specific outcome for tissue engineering applications.

3.6 Methods

Chemical vapor deposition (CVD) Graphene film growth and transfer

Graphene was grown on copper (Cu) foil (99.8% Alfa Aesar 0.5 mm) utilizing methane (CH₄) as a carbon source, similar to previously reported methods.⁷⁹ Briefly, Cu

foil was placed in a custom-built 1" tube CVD system.⁸⁰ The system was put under vacuum and then brought to 1 atm with a continuous argon (Ar) flow of 1000 sccm while the system heated to 1000 °C. The Cu foil was then annealed in an Ar (800 sccm) and hydrogen (H₂) (200 sccm) flow for 90 minutes while maintaining 1 atm. To induce graphene growth, the gas switches to CH₄ (500 sccm) and H₂ (300 sccm) for 90 minutes at 1000 °C. The resulting graphene/Cu was then cooled to room temperature under Ar gas flow of 500 sccm and coated with two different layers of poly (methyl methacrylate (PMMA) to preserve graphene integrity during the transfer process. Both 495 K PMMA A2 and 950 K PMMA A4 were used respectively to coat the graphene and were baked for 2 minutes at 200°C following each coating. To remove the PMMA/graphene from the Cu foil, the Cu foil was used as a working electrode for electrochemical delamination.⁷⁹ The Cu foil was gradually immersed in a 0.6 M NaOH electrolyte solution at a 45° angle which contained a platinum mesh counter electrode and an Ag/AgCl reference electrode. A -2.1 mV voltage was applied. Once detached, the PMMA/graphene films underwent numerous nano pure water rinses before transferring to a 25.4 × 25.4 mm² quartz glass coverslips. The PMMA was then removed using an acetone bath. Lastly, the resultant graphene/quartz glass composites were annealed at 500°C for 30 minutes under Ar gas flow.

Graphene Ink Synthesis and Printing

Based on our previous methods, we produced graphene ink by solvent assisted exfoliation of bulk graphite powder.⁸¹ Graphene flakes were obtained by sonicating bulk graphite powder (50 mg/mL) and 2% ethyl cellulose (EC) in ethanol for 90 minutes. The graphene/EC was then centrifuged at 4500 RPM for 60 minutes to remove any remaining

graphite and the supernatant was immediately collected. An aqueous solution of NaCl (40 mg/mL; Sigma-Aldrich, >99.5%) was added to the supernatant and centrifuged at 4500 RPM for 15 minutes to collect the graphene. The resulting graphene/EC was then transferred to a PTEE (Teflon) plate and dried overnight. To formulate an ink for inkjet printing (IJP), the dried graphene/EC was then sonicated in a mixture of 92.5% cyclohexanone and 7.5% terpineol solution for 30 minutes. The mixture was then centrifuged at 4500 RPM for 15 minutes to remove any non-dispersed flakes and the supernatant was collected. The resulting graphene ink (3.5 mg/mL) was printed onto glass coverslips using a Dimatix/Fujifilm 2850 IJP system. Graphene was printed using 10 print passes and baked at 350 °C for 20 minutes to remove solvents and residual polymers.

Epitaxial Graphene Growth on SiC

Epitaxial graphene on SiC was obtained via thermal decomposition of SiC. The SiC samples were held at 1250 °C of on-axis 4H-SiC (0001) in Ar atmosphere to remove Si and obtain the graphene.¹⁵ To obtain quasi-free-standing monolayer graphene, hydrogen intercalation of the buffer layer occurred at 900 °C, at atmospheric pressure, in molecular hydrogen. Sample dimensions were 6 × 6 mm².

Materials Characterization.

Atomic Force Microscopy

PeakForce tapping mode AFM imaging was performed on the three different graphene bioscaffolds samples using a Bruker Dimension FastScan AFM. Surface topography was mapped using a ScanAsyst-Air- HR probe (Bruker, $k = 0.4$ N/m, 2 nm radius of curvature) and a ~2 nN Peakforce setpoint. A 10 μm x 10 μm AFM scan with a

resolution 1024 x 1024 and pixel size of ~10 nm was collected on each sample. Image processing and surface roughness analysis were conducted using NanoScope Analysis Version 1.90 (Bruker). All topographical images were processed with an XY plane fit to remove sample tip and tilt, followed by a first order flatten to remove any line-to-line offsets. The average roughness (Ra) of each image was found using the Nanoscope software. Nanoindentation was used to determine stiffness and Young's modulus.

Raman spectroscopy

A Horiba Lab RAM HR Evolution Raman microscope was used to collect Raman spectral data on the three graphene bioscaffolds. A 633 nm He:Ne laser was used in conjunction with a 100x objective, 1800 gr/mm grating, 70 μm aperture, and 50% filter to collect spectra from 1,300-3,000 cm^{-1} on a random 100 μm^2 area of each bioscaffold. The resulting Raman peaks were fit using LabSpec6 software.

Cell Culture

Agarose gel (1%) was applied to the bottom of the 6-well plates and on the border of the three graphene scaffolds to prevent cells from migrating off the bioscaffolds during the experiment and influencing results. The bioscaffolds were sterilized using UV irradiation for one hour. C2C12 (ATCC) bipotential myoblast cells were cultured in DMEM growth media containing 10% fetal bovine serum and 1% penicillin/streptomycin in 5% CO_2 at 37°C. As controls, C2C12 cells were also cultured on the three different substrates (quartz, SiC, and glass). Each graphene bioscaffold and controls were seeded with approximately 13,000 cells/ cm^2 . Cells were then cultured as indicated above and the DMEM was exchanged every two days. On day 7, the samples were then prepared for imaging or genetic analysis. For imaging analysis, viable cells were stained using

Calcein-AM and imaged using an EVOS Cell Imaging System (ThermoFisher Scientific) to investigate morphology. Aspect ratio was determined to quantify cell shape using methods of Wang et al. by measuring the longest length of the cell structure and the shortest width.⁷⁷ Cell alignment for each bioscaffold was quantified to calculate a k value using FiberFit software (<https://www.boisestate.edu/coen-ntm/technology/fiberfit/>). ImageJ was used to preprocess the six images taken of the C2C12 cells on the six bioscaffolds and converted into 8-bit images for FiberFit preprocessing requirements.⁷⁸ The more alignment seen in the images, the larger the k-value and the less alignment seen, the smaller the k-value.⁷⁸ FiberFit also provided fiber orientation (μ), sigma and R^2 values.

qPCR

RNA from each sample was extracted following the TRIzol protocol for RNA extraction (Thermo Fisher Scientific). RNA concentration was determined by measuring the absorbance at 260 nm. The RT² First Strand Kit (Qiagen) was used for the generation of cDNA. Qiagen kits used were specific to myogenesis and the extracellular matrix. Genes were amplified by RT-qPCR using a Roche Lightcycler 96 (Roche).

Housekeeping gene (HKG) analysis.

The gene expression results were normalized to the average of the housekeeping genes *actb*, encoding Actin, cytoplasmic 1, and *gapdh*, encoding glyceraldehyde 3-phosphate dehydrogenase. This was determined using a house-keeping gene analysis from previously established protocols.⁷⁰ These two genes were selected as the housekeeping genes based on comparison to three other candidates (*b2m*, *hsp90ab1*, and *gusb*). *Actb* and *gapdh* were found to be stably expressed based on minimal variance. For

this panel of thirty-one genes, the normalized $2^{-(\Delta Ct)}$ values were calculated. Using the $2^{-(\Delta Ct)}$ method, we were able to determine relative abundance of gene expression compared to a positive control threshold. The positive controls were C2C12 cells grown on the base scaffolds: silicon carbide, quartz, and glass.

3.7 Supporting figures and tables

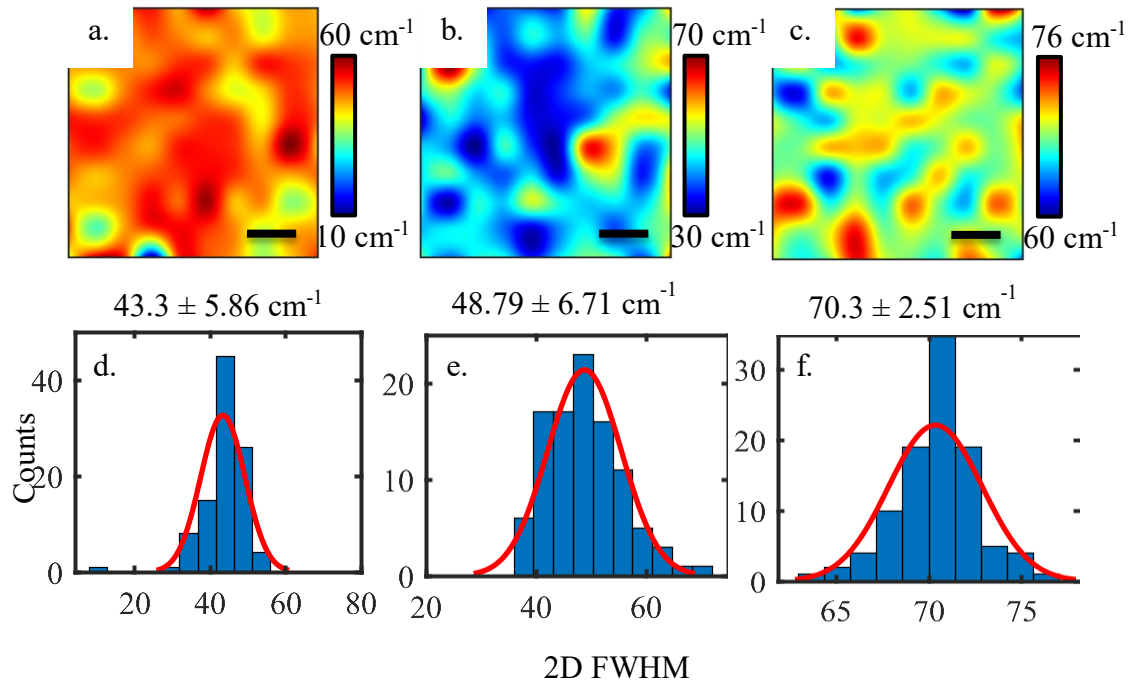


Figure 3.6 2D FWHM for all graphene bioscaffolds represented in Raman spectra maps where a) is CVD, b) epitaxial, and c) printed graphene and histograms of these positions where d) is CVD, e) epitaxial, and f) printed graphene

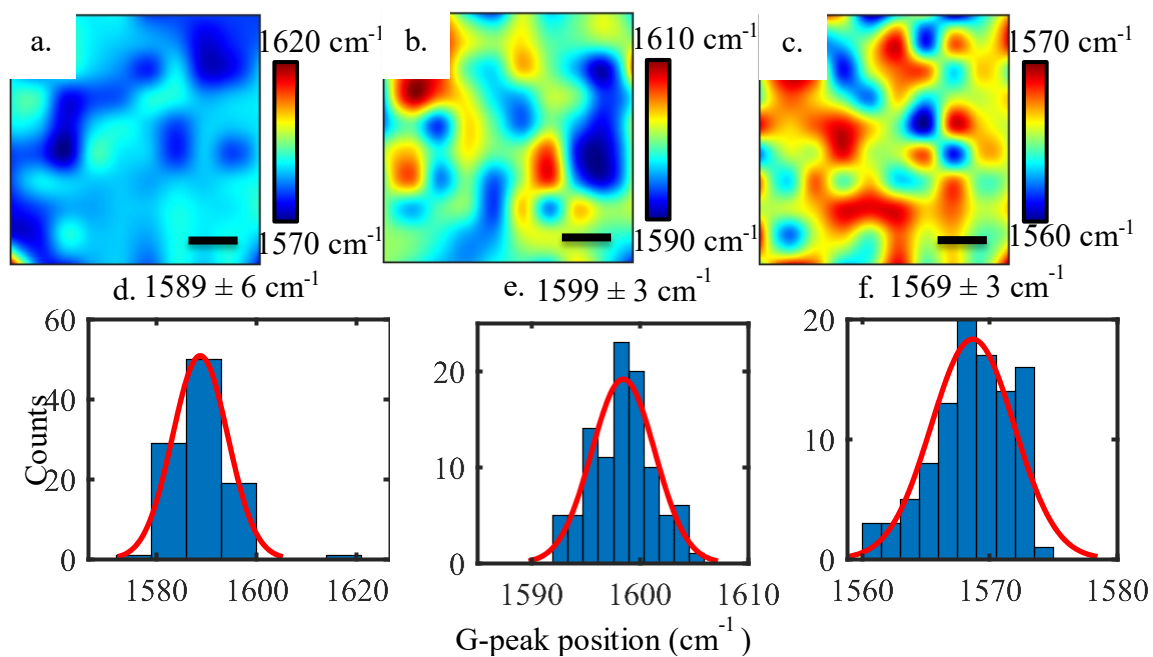


Figure 3.7 G-peak position for all graphene bioscaffolds represented in Raman spectra maps where a) is CVD, b) epitaxial, and c) printed graphene and histograms of these positions where d) is CVD, e) epitaxial, and f) printed graphene

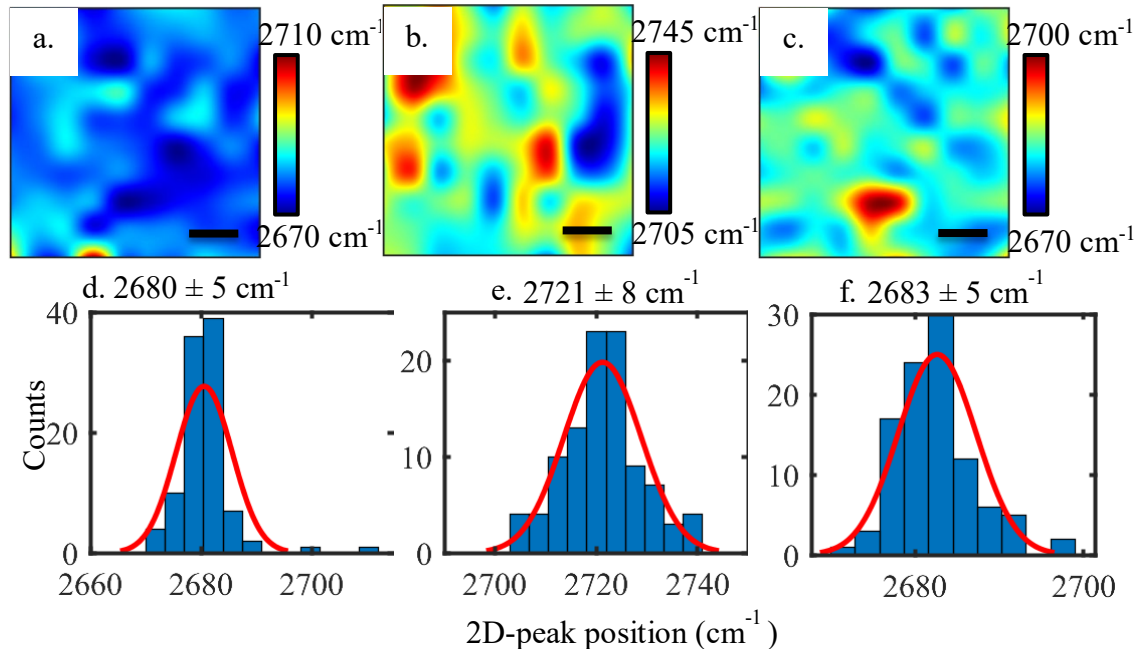


Figure 3.8 2D-peak position for all graphene bioscaffolds represented in Raman spectra maps where a) is CVD, b) epitaxial, and c) printed graphene and histograms of these positions where d) is CVD, e) epitaxial, and f) printed graphene

Table 3.1 Genes relating to myogenesis

	Gene symbol	Protein name	Function in Myogenesis	Ref
1	Des	Desmin	Involved in maintenance of sarcomeres, inter-connecting the Z-disks and forming fibrils.	82, 83, 89
2	Dmpk	DM1 Protein Kinase	Necessary for myogenin expression in differentiating C2C12 cells	82, 84
3	Musk	Muscle, skeletal receptor tyrosine-protein kinase	Receptor tyrosine kinase – plays a central role in formation and maintenance of neuromuscular junction (NMJ).	82, 85
4	Myod1	Myogenic differentiation 1	Acts as a transcriptional activator that promotes transcription of muscle-specific target genes and plays a role in muscle differentiation	82, 86
5	Myog	Myogenin	Acts as a transcriptional activator that promotes transcription of muscle-specific target genes and plays a role in muscle differentiation, cell cycle exit and muscle atrophy.	82, 87, 89
6	Utrn	Utrophin	Binds to dystroglycan	82, 88

Table 3.2 Genes relating to contractility

	Gene symbol	Protein name	Function in Myogenesis	Ref
1	Acta1	Actin alpha 1	Involved in various types of cell motility	82
2	Actn3	Alpha-actinin 3	Involved in assembly and maintenance of muscle fibers	82
3	Atp2a1	Sarcoplasmic/endoplasmic reticulum calcium ATPase	Key regulator in performance of striated m	82
4	Tnnc1	Troponin C1, slow skeletal and cardiac type	Troponin is the central regulatory protein of striated muscle contraction	82, 89
5	Tnni2	Troponin I2, fast skeletal type	Troponin I is the inhibitory subunit of troponin, the thin filament regulatory complex which confers calcium-sensitivity to striated muscle actomyosin ATPase activity	82, 90
6	Tnnt1	Troponin T1, slow skeletal type	Important for muscle contraction; binds to tropomyosin	82
7	Ttn	Titin	Key component for vertebrate striated muscle assembly and function	82

Table 3.3 Genes relating to the ECM

	Gene symbol	Protein name	Function in Myogenesis	Ref
1	Colla1	Collagen alpha 1	Fibrillar forming collagen	82
2	Col3a1	Collagen type 3 Alpha 1 chain	Involved in regeneration of cortical development	82
3	Lamb2	Laminin subunit beta 2	Regulates formation of motor nerve terminals	82
4	Postn	Periostin	Induces cell attachment and spreading and plays a role in cell adhesion	82
5	Tnc	Tenascin C	ECM protein implicated in guidance of migrating neurons as well as axons during development, synaptic plasticity and neuronal regeneration	82

Table 3.4 Genes relating to attachment

	Gene symbol	Protein name	Function in Myogenesis	Ref
1	Ncam1	Neural cell adhesion molecule 1	Cell adhesion molecule involved in neuron-neuron adhesion	82
2	Sgce	Sarcoglycan epsilon	Component of sarcoglycan complex, a subcomplex of dystrophin-glycoprotein complex which forms a link between the F-actin cytoskeleton and ECM	82
3	Spp1	Secreted phosphoprotein 1	Major non-collagenous bone protein that binds tightly to hydroxyapatite	82
4	Vcan	Versican	May play a role in intercellular signaling and in connecting cells with the ECM	82

Table 3.5 Genes relating to ECM remodeling

	Gene symbol	Protein name	Function in Myogenesis	Ref
1	Adamts2	ADAM Metallopeptidase With Thrombospondin Type 1 Motif 2	Cleaves propeptides of type I and II collagen prior to fibril assembly	82
2	Mmp9	Matrix Metallopeptidase 9	Plays an essential role in local proteolysis of the ECM and leukocyte migration	82, 91
3	Timp1	Tissue Inhibitor of Metalloproteinases 1	Inhibitor of Mmps and Adamts	82
4	Timp2	Tissue Inhibitor of Metalloproteinases 2	Inhibitor of Mmps and Adamts	82, 92

CHAPTER 4: CONCLUSION

4.1 Summary

The research goals of this study were to show that graphene production methods result in differences in graphene's structure and properties, and that these differences are reflected in how graphene performs as a bioscaffold. Three graphene bioscaffolds were produced each by different synthesis methods. Roughness, stiffness, and electronic nature was characterized for each prior to cell culture. C2C12 cells, murine muscle cells, were subcultured until passage four before seeded on the graphene bioscaffolds and their respective controls. The cells were seeded on each of the graphene bioscaffolds (and respective controls) at the same cell density, on the same day (day 0) and were allowed to culture for seven days under the same growth conditions, 5% CO₂ in an incubator set to 37°C. Finally, the cell morphology and gene expression were studied and compared to determine how the three graphene bioscaffolds performed.

Key findings include:

- Each graphene synthesis method resulted in different roughness, stiffness, and electronic properties
- C2C12 cell morphology and gene expression were different on each bioscaffold on the seventh day of cell culture
- Cell morphology structures seen for the CVD graphene bioscaffold was the only graphene bioscaffold which presented muscle-like

structures. Epitaxial and printed graphene bioscaffolds presented bone-like structures suggesting a possible shift in cell pathway

- Different gene profiles were produced for each graphene bioscaffold.

Different gene profiles and morphological structures are seen for graphene scaffolds produced using three different methods. These results could prove useful when deciding which type of graphene method to use if one were trying to get a specific outcome. If electrical stimulation of graphene were to be explored, knowing which graphene synthesis method would best suit the target tissue would be useful. Many gene pathways exist, and many genes exist. Many gene pathways can lead to muscle.

4.2 Limitations

Limitations in this study include sample preparation, sample characterization methods, and biochemical analysis. Each graphene bioscaffold had its own control substrates. Epitaxial graphene was grown directly on 1 cm x 1 cm SiC samples, whereas the CVD graphene was transferred from 2.54 cm x 2.54 cm Cu foil onto 2.54 cm x 2.54 cm quartz glass via electrochemical delamination and the graphene ink acquired by solvent assisted exfoliation of graphite was printed in 1 cm x 1 cm squares onto 2.54 cm x 2.54 cm glass coverslips. To ensure as many cells attached to the graphene and that as little interference between the graphene and cell interaction and the area in which the cells were to be seeded on were of similar dimensions, agarose was used to cover the tissue culture dishes, exposed base substrates of the graphene and their respective controls. Although effective in keeping the cells on the substrates, agarose was difficult to apply.

The graphene ink had initially been printed on quartz, however, once cells were seeded on these samples, the printed graphene detached from the quartz and broke into pieces rendering the samples unusable. The graphene ink was then printed on glass coverslips which remained intact after seeding cells and for the duration of the seven-day experiment. Having the graphene bioscaffolds integrated on three different base substrates meant that there needed to be three different control substrates. This introduced variables which needed to be accounted for as the C2C12 cell growth on the control substrates reflected different morphologies. Instead of making comparisons between the graphene alone, the base substrates needed to be included in the system and when looking at gene expression, more steps needed to be added to ensure that we were solely comparing the graphene alone.

The Stiffness measurements collected revealed values which correlated to the underlying base substrate. This caused inaccuracies in the stiffness measurements as the base substrates may have been too hard to get an accurate stiffness measurement of the graphene alone.

Biochemical analysis is important in accessing how graphene performs as a bioscaffold, it is as equally important when comparing the performances and correlating differences seen to the structure and properties obtained by the different processes. As reflected in the morphology, the three graphene substrates revealed more than one phenotype. In addition to using the ECM and muscle assays to study the gene expression in each bioscaffold, including a bone assay would have also been useful in obtaining a better understanding of what was happening to the cells.

There is a direct correlation seen between the graphene processing methods and the structure and properties each possess. This study shows that these correlations impact how graphene performs as a bioscaffold by producing different morphological cell structures as well as different genetic profiles.

4.3 Future work

In continuation to this study, further exploration of graphene's electrical properties is warranted and could answer questions regarding graphene charge type (n-type or p-type) and the effect it has on cells. Performing transmembrane potential studies on the different graphene types could potentially determine if difference in graphene doping has an impact on cell growth and differentiation. This study has the potential to serve as a preliminary study for another future direction, which involves applying an electrical stimulus to graphene to guide cell differentiation.

It is known that cell differentiation is influenced by electrical stimuli, but an area which lacks information is the ability to create more than one tissue type from one cell line in one cell culture dish. Exploring the possibility of applying two different voltages to two sections (one voltage per section) of a graphene bioscaffold, simultaneously, could produce produces more than one tissue type. Lastly, repeating these studies using hMSCs, with the goal of creating any type of tissue would be beneficial knowledge throughout the entire tissue engineering community not only the musculoskeletal tissue engineering community.

REFERENCES

- (1) Grzelkowska-Kowalczyk, K. The Importance of Extracellular Matrix in Skeletal Muscle Development and Function. In *Composition and Function of the Extracellular Matrix in the Human Body*, InTech, 2016.
- (2) Carnes, M. E.; Pins, G. D. Skeletal Muscle Tissue Engineering: Biomaterials-Based Strategies for the Treatment of Volumetric Muscle Loss. *Bioengineering* **2020**, *7* (3), 85. DOI: 10.3390/bioengineering7030085 (accessed 2022-07-06T17:14:23).
- (3) March, L.; Smith, E. U. R.; Hoy, D. G.; Cross, M. J.; Sanchez-Riera, L.; Blyth, F.; Buchbinder, R.; Vos, T.; Woolf, A. D. Burden of disability due to musculoskeletal (MSK) disorders. *Best Practice & Research Clinical Rheumatology* **2014**, *28* (3), 353-366. DOI: 10.1016/j.berh.2014.08.002 (accessed 2022-05-16T23:34:53).
- (4) Rossi, C. A.; Pozzobon, M.; De Coppi, P. Advances in musculoskeletal tissue engineering. *Organogenesis* **2010**, *6* (3), 167-172. DOI: 10.4161/org.6.3.12419 (accessed 2022-09-01T18:06:32).
- (5) Dzobo, K.; Thomford, N. E.; Senthebane, D. A.; Shipanga, H.; Rowe, A.; Dandara, C.; Pillay, M.; Motaung, K. S. C. M. Advances in Regenerative Medicine and Tissue Engineering: Innovation and Transformation of Medicine. *Stem Cells International* **2018**, *2018*, 1-24. DOI: 10.1155/2018/2495848 (accessed 2022-08-31T02:36:25).
- (6) Maras, M. A. J.; Rahman, S. F.; Hardi, G. W. Progressive graphene derivatives scaffold based for tissue engineering application: A review. In *THE 5TH BIOMEDICAL ENGINEERING'S RECENT PROGRESS IN BIOMATERIALS, DRUGS DEVELOPMENT, AND MEDICAL DEVICES: Proceedings of the 5th International Symposium of Biomedical Engineering (ISBE) 2020*, 2021.

- (7) Kim, Y.; Ko, H.; Kwon, I. K.; Shin, K. Extracellular Matrix Revisited: Roles in Tissue Engineering. *Int Neurourol J* **2016**, *20* (Suppl 1), S23-S29. DOI: 10.5213/inj.1632600.318 PubMed.
- (8) Yocham, K. M.; Scott, C.; Fujimoto, K.; Brown, R.; Tanasse, E.; Oxford, J. T.; Lujan, T. J.; Estrada, D. Mechanical Properties of Graphene Foam and Graphene Foam-Tissue Composites. *Advanced Engineering Materials* **2018**, *20* (9), 1800166. DOI: 10.1002/adem.201800166 (accessed 2022-07-07T17:31:39). Crowder, S. W.; Prasai, D.; Rath, R.; Balikov, D. A.; Bae, H.; Bolotin, K. I.; Sung, H.-J. Three-dimensional graphene foams promote osteogenic differentiation of human mesenchymal stem cells. *Nanoscale* **2013**, *5* (10), 4171. DOI: 10.1039/c3nr00803g (accessed 2022-06-28T16:28:35).
- (9) Zhang, Z.; Klausen, L. H.; Chen, M.; Dong, M. Electroactive Scaffolds for Neurogenesis and Myogenesis: Graphene-Based Nanomaterials. *Small* **2018**, *14* (48), e1801983. DOI: 10.1002/smll.201801983 From NLM Medline. Xie, H.; Cao, T.; Viana Gomes, J.; Castro Neto, A.; Rosa, V. Two and three-dimensional graphene substrates to magnify osteogenic differentiation of periodontal ligament stem cells. *Carbon* **2015**, *93*. DOI: 10.1016/j.carbon.2015.05.071.
- (10) Kim, J.; Leem, J.; Kim, H. N.; Kang, P.; Choi, J.; Haque, M. F.; Kang, D.; Nam, S. Uniaxially crumpled graphene as a platform for guided myotube formation. *Microsystems & Nanoengineering* **2019**, *5* (1). DOI: 10.1038/s41378-019-0098-6 (accessed 2022-06-28T16:30:05).
- (11) Xie, H.; Cao, T.; Franco-Obregón, A.; Rosa, V. Graphene-Induced Osteogenic Differentiation Is Mediated by the Integrin/FAK Axis. *International Journal of Molecular Sciences* **2019**, *20* (3), 574. DOI: 10.3390/ijms20030574 (accessed 2022-06-28T16:51:21).
- (12) Xie, H.; Chua, M.; Islam, I.; Bentini, R.; Cao, T.; Viana-Gomes, J. C.; Castro Neto, A. H.; Rosa, V. CVD-grown monolayer graphene induces osteogenic but not odontoblastic differentiation of dental pulp stem cells. *Dent Mater* **2017**, *33* (1), e13-e21. DOI: 10.1016/j.dental.2016.09.030 From NLM.

- (13) Bajaj, P.; Rivera, J. A.; Marchwiany, D.; Solovyeva, V.; Bashir, R. Graphene-based patterning and differentiation of C2C12 myoblasts. *Advanced healthcare materials* **2014**, *3* (7), 995-1000.
- (14) Convertino, D.; Fabbri, F.; Mishra, N.; Mainardi, M.; Cappello, V.; Testa, G.; Capsoni, S.; Albertazzi, L.; Luin, S.; Marchetti, L.; et al. Graphene Promotes Axon Elongation through Local Stall of Nerve Growth Factor Signaling Endosomes. *Nano Lett* **2020**, *20* (5), 3633-3641. DOI: 10.1021/acs.nanolett.0c00571 From NLM Medline.
- (15) Convertino, D.; Luin, S.; Marchetti, L.; Coletti, C. Peripheral Neuron Survival and Outgrowth on Graphene. *Frontiers in Neuroscience* **2018**, *12*, Original Research. DOI: 10.3389/fnins.2018.00001.
- (16) Singh, V.; Joung, D.; Zhai, L.; Das, S.; Khondaker, S. I.; Seal, S. Graphene based materials: Past, present and future. *Progress in Materials Science* **2011**, *56* (8), 1178-1271. DOI: 10.1016/j.pmatsci.2011.03.003.
- (17) Lee, S. K.; Kim, H.; Shim, B. S. Graphene: an emerging material for biological tissue engineering. *Carbon letters* **2013**, *14* (2), 63-75. DOI: 10.5714/cl.2013.14.2.063.
- (18) Kim, J.; Leem, J.; Kim, H. N.; Kang, P.; Choi, J.; Haque, M. F.; Kang, D.; Nam, S. Uniaxially crumpled graphene as a platform for guided myotube formation. *Microsystems & nanoengineering* **2019**, *5* (1), 1-10.
- (19) Kim, S. J.; Cho, K. W.; Cho, H. R.; Wang, L.; Park, S. Y.; Lee, S. E.; Hyeon, T.; Lu, N.; Choi, S. H.; Kim, D.-H. Stretchable and Transparent Biointerface Using Cell-Sheet-Graphene Hybrid for Electrophysiology and Therapy of Skeletal Muscle. *Advanced Functional Materials* **2016**, *26*. DOI: 10.1002/adfm.201504578.
- (20) Kim, T.; Kahng, Y. H.; Lee, T.; Lee, K.; Kim, D. H. Graphene films show stable cell attachment and biocompatibility with electrogenic primary cardiac cells. *Molecules and Cells* **2013**, *36* (6), 577-582. DOI: 10.1007/s10059-013-0277-5 (accessed 2022-02-03T17:46:03).

- (21) Shin, S. R.; Li, Y.-C.; Jang, H. L.; Khoshakhlagh, P.; Akbari, M.; Nasajpour, A.; Zhang, Y. S.; Tamayol, A.; Khademhosseini, A. Graphene-based materials for tissue engineering. *Advanced Drug Delivery Reviews* **2016**, *105*, 255-274. DOI: 10.1016/j.addr.2016.03.007 (accessed 2022-07-09T04:25:17).
- (22) Gu, M.; Lv, L.; Du, F.; Niu, T.; Chen, T.; Xia, D.; Wang, S.; Zhao, X.; Liu, J.; Liu, Y.; et al. Effects of thermal treatment on the adhesion strength and osteoinductive activity of single-layer graphene sheets on titanium substrates. *Scientific Reports* **2018**, *8* (1). DOI: 10.1038/s41598-018-26551-w (accessed 2022-06-28T16:41:05).
- (23) Kitko, K. E.; Hong, T.; Lazarenko, R. M.; Ying, D.; Xu, Y.-Q.; Zhang, Q. Membrane cholesterol mediates the cellular effects of monolayer graphene substrates. *Nature Communications* **2018**, *9* (1). DOI: 10.1038/s41467-018-03185-0 (accessed 2022-01-29T20:28:17).
- (24) Novoselov, K. S.; Geim, A. K.; Morozov, S. V.; Jiang, D.; Katsnelson, M. I.; Grigorieva, I. V.; Dubonos, S. V.; Firsov, A. A. Two-dimensional gas of massless Dirac fermions in graphene. *Nature* **2005**, *438* (7065), 197-200. DOI: 10.1038/nature04233 (accessed 2022-07-31T22:42:58).
- (25) Balandin, A. A.; Ghosh, S.; Nika, D. L.; Pokatilov, E. P. Thermal Conduction in Suspended Graphene Layers. *Fullerenes, Nanotubes and Carbon Nanostructures* **2010**, *18* (4-6), 474-486. DOI: 10.1080/1536383x.2010.487785.
- (26) Lee, C.; Wei, X.; Kysar, J. W.; Hone, J. Measurement of the elastic properties and intrinsic strength of monolayer graphene. *Science* **2008**, *321* (5887), 385-388. DOI: 10.1126/science.1157996 From NLM PubMed-not-MEDLINE.
- (27) Rudrapati, R. Graphene: Fabrication Methods, Properties, and Applications in Modern Industries. In *Graphene Production and Application*, IntechOpen, 2020.
- (28) Kumar, V.; Kumar, A.; Lee, D.-J.; Park, S.-S. Estimation of Number of Graphene Layers Using Different Methods: A Focused Review. *Materials* **2021**, *14* (16), 4590. DOI: 10.3390/ma14164590.

- (29) Raslan, A.; Saenz Del Burgo, L.; Ciriza, J.; Pedraz, J. L. Graphene oxide and reduced graphene oxide-based scaffolds in regenerative medicine. *Int J Pharm* **2020**, *580*, 119226. DOI: 10.1016/j.ijpharm.2020.119226 From NLM Medline.
- (30) Kalbacova, M.; Broz, A.; Kong, J.; Kalbac, M. Graphene substrates promote adherence of human osteoblasts and mesenchymal stromal cells. *Carbon* **2010**, *48* (15), 4323-4329. DOI: <https://doi.org/10.1016/j.carbon.2010.07.045>.
- (31) Nayak, T. R.; Andersen, H.; Makam, V. S.; Khaw, C.; Bae, S.; Xu, X.; Ee, P.-L. R.; Ahn, J.-H.; Hong, B. H.; Pastorin, G.; et al. Graphene for Controlled and Accelerated Osteogenic Differentiation of Human Mesenchymal Stem Cells. *ACS Nano* **2011**, *5* (6), 4670-4678. DOI: 10.1021/nm200500h (accessed 2022-06-28T16:29:22).
- (32) Hernaez, M.; Zamarreño, C.; Melendi-Espina, S.; Bird, L.; Mayes, A.; Arregui, F. Optical Fibre Sensors Using Graphene-Based Materials: A Review. *Sensors* **2017**, *17* (12), 155. DOI: 10.3390/s17010155 (accessed 2022-11-08T05:56:15).
- (33) Feng, C.; Zhu, D.; Wang, Y.; Jin, S. Electromechanical Behaviors of Graphene Reinforced Polymer Composites: A Review. *Materials (Basel)* **2020**, *13* (3). DOI: 10.3390/ma13030528 From NLM PubMed-not-MEDLINE.
- (34) Bonaccorso, F.; Lombardo, A.; Hasan, T.; Sun, Z.; Colombo, L.; Ferrari, A. C. Production and processing of graphene and 2d crystals. *Materials Today* **2012**, *15* (12), 564-589. DOI: 10.1016/s1369-7021(13)70014-2.
- (35) Pandhi, T.; Cornwell, C.; Fujimoto, K.; Barnes, P.; Cox, J.; Xiong, H.; Davis, P. H.; Subbaraman, H.; Koehne, J. E.; Estrada, D. Fully inkjet-printed multilayered graphene-based flexible electrodes for repeatable electrochemical response. *RSC Advances* **2020**, *10* (63), 38205-38219. DOI: 10.1039/d0ra04786d (accessed 2022-10-15T19:35:21).
- (36) Stanford, M. G.; Zhang, C.; Fowlkes, J. D.; Hoffman, A.; Ivanov, I. N.; Rack, P. D.; Tour, J. M. High-Resolution Laser-Induced Graphene. Flexible Electronics beyond the Visible Limit. *ACS Appl Mater Interfaces* **2020**, *12* (9), 10902-10907. DOI: 10.1021/acsami.0c01377 From NLM PubMed-not-MEDLINE.

- (37) Liu, Z.; Liu, W.; Xie, X.; Zhao, W.; Wen, Y.; Wang, Q.; Ou, B. Lateral Size of Graphene Characterized by Atomic Force Microscope. *IOP Conference Series: Earth and Environmental Science* **2019**, *252*. DOI: 10.1088/1755-1315/252/2/022022. Webb, H. K.; Truong, V. K.; Hasan, J.; Fluke, C.; Crawford, R. J.; Ivanova, E. P. Roughness Parameters for Standard Description of Surface Nanoarchitecture. *Scanning* **2012**, *34* (4), 257-263. DOI: <https://doi.org/10.1002/sca.21002>.
- (38) Enriques, A. E.; Howard, S.; Timsina, R.; Khadka, N. K.; Hoover, A. N.; Ray, A. E.; Ding, L.; Onwumelu, C.; Nordeng, S.; Mainali, L.; et al. Atomic Force Microscopy Cantilever-Based Nanoindentation: Mechanical Property Measurements at the Nanoscale in Air and Fluid. *J Vis Exp* **2022**, (190). DOI: 10.3791/64497 From NLM Medline.
- (39) Ferrari, A. C. Raman spectroscopy of graphene and graphite: Disorder, electron-phonon coupling, doping and nonadiabatic effects. *Solid State Communications* **2007**, *143* (1-2), 47-57. DOI: 10.1016/j.ssc.2007.03.052. Malard, L. M.; Pimenta, M. A.; Dresselhaus, G.; Dresselhaus, M. S. Raman spectroscopy in graphene. *Physics Reports* **2009**, *473* (5-6), 51-87. DOI: 10.1016/j.physrep.2009.02.003.
- (40) Borghi, F. F.; Bean, P. A.; Evans, M. D. M.; Van Der Laan, T.; Kumar, S.; Ostrikov, K. Nanostructured Graphene Surfaces Promote Different Stages of Bone Cell Differentiation. *Nano-Micro Letters* **2018**, *10* (3). DOI: 10.1007/s40820-018-0198-0 (accessed 2022-01-06T03:09:30).
- (41) Lee, D. S.; Riedl, C.; Krauss, B.; Von Klitzing, K.; Starke, U.; Smet, J. H. Raman Spectra of Epitaxial Graphene on SiC and of Epitaxial Graphene Transferred to SiO₂. *Nano Letters* **2008**, *8* (12), 4320-4325. DOI: 10.1021/nl802156w (accessed 2022-07-31T21:42:02).

- (42) Das, A.; Chakraborty, B.; Sood, A. K. Raman spectroscopy of graphene on different substrates and influence of defects. *Bulletin of Materials Science* **2008**, *31* (3), 579-584. DOI: 10.1007/s12034-008-0090-5 (accessed 2021-12-15T17:05:00).
Hao, Y.; Wang, Y.; Wang, L.; Ni, Z.; Wang, Z.; Wang, R.; Koo, C. K.; Shen, Z.; Thong, J. T. Probing layer number and stacking order of few-layer graphene by Raman spectroscopy. *Small* **2010**, *6* (2), 195-200. DOI: 10.1002/sml.200901173
From NLM Medline.
- (43) Das, A.; Pisana, S.; Chakraborty, B.; Piscanec, S.; Saha, S. K.; Waghmare, U. V.; Novoselov, K. S.; Krishnamurthy, H. R.; Geim, A. K.; Ferrari, A. C.; et al. Monitoring dopants by Raman scattering in an electrochemically top-gated graphene transistor. *Nat Nanotechnol* **2008**, *3* (4), 210-215. DOI: 10.1038/nnano.2008.67 From NLM Medline.
- (44) Lee, J. E.; Ahn, G.; Shim, J.; Lee, Y. S.; Ryu, S. Optical separation of mechanical strain from charge doping in graphene. *Nature Communications* **2012**, *3* (1), 1024. DOI: 10.1038/ncomms2022 (accessed 2022-11-16T17:52:21). Neumann, C.; Reichardt, S.; Venezuela, P.; Drögeler, M.; Banszerus, L.; Schmitz, M.; Watanabe, K.; Taniguchi, T.; Mauri, F.; Beschoten, B.; et al. Raman spectroscopy as probe of nanometre-scale strain variations in graphene. *Nature Communications* **2015**, *6* (1), 8429. DOI: 10.1038/ncomms9429 (accessed 2022-11-16T17:53:33).
- (45) Casiraghi, C.; Pisana, S.; Novoselov, K. S.; Geim, A. K.; Ferrari, A. C. Raman fingerprint of charged impurities in graphene. *Applied Physics Letters* **2007**, *91* (23), 233108. DOI: 10.1063/1.2818692 (accessed 2021-12-15T17:05:47).
- (46) Ahadian, S. Electrically regulated differentiation of skeletal muscle cells on ultrathin graphene-based films. *RSC Advances* **2014**, *4*.
- (47) Kalbacova, M. H.; Verdanova, M.; Broz, A.; Vetushka, A.; Fejfar, A.; Kalbac, M. Modulated surface of single-layer graphene controls cell behavior. *Carbon* **2014**, *72*, 207-214. DOI: <https://doi.org/10.1016/j.carbon.2014.02.004>.

- (48) Lee, W. C.; Lim, C. H. Y. X.; Shi, H.; Tang, L. A. L.; Wang, Y.; Lim, C. T.; Loh, K. P. Origin of Enhanced Stem Cell Growth and Differentiation on Graphene and Graphene Oxide. *ACS Nano* **2011**, 5 (9), 7334-7341. DOI: 10.1021/nn202190c (accessed 2022-06-28T16:38:38).
- (49) Aryaei, A.; Jayatissa, A. H.; Jayasuriya, A. C. The effect of graphene substrate on osteoblast cell adhesion and proliferation. *Journal of Biomedical Materials Research Part A* **2014**, 102 (9), 3282-3290. DOI: 10.1002/jbm.a.34993 (accessed 2022-06-28T16:40:23).
- (50) Balikov, D. A.; Fang, B.; Chun, Y. W.; Crowder, S. W.; Prasai, D.; Lee, J. B.; Bolotin, K. I.; Sung, H.-J. Directing lineage specification of human mesenchymal stem cells by decoupling electrical stimulation and physical patterning on unmodified graphene. *Nanoscale* **2016**, 8 (28), 13730-13739. DOI: 10.1039/c6nr04400j (accessed 2022-05-16T23:18:57).
- (51) Xie, H.; Cao, T.; Gomes, J. V.; Castro Neto, A. H.; Rosa, V. Two and three-dimensional graphene substrates to magnify osteogenic differentiation of periodontal ligament stem cells. *Carbon* **2015**, 93, 266-275. DOI: <https://doi.org/10.1016/j.carbon.2015.05.071>.
- (52) Li, Z.; Xiang, S.; Li, E. N.; Fritch, M. R.; Alexander, P. G.; Lin, H.; Tuan, R. S. Tissue Engineering for Musculoskeletal Regeneration and Disease Modeling. *Handb Exp Pharmacol* **2021**, 265, 235-268. DOI: 10.1007/164_2020_377 From NLM Medline.
- (53) Florencio-Silva, R.; Sasso, G. R. D. S.; Sasso-Cerri, E.; Simões, M. J.; Cerri, P. S. Biology of Bone Tissue: Structure, Function, and Factors That Influence Bone Cells. *BioMed Research International* **2015**, 2015, 1-17. DOI: 10.1155/2015/421746 (accessed 2022-10-07T17:51:42).
- (54) Le, B. Q.; and Nurcombe, V. a. C., Simon McKenzie and Van Blitterswijk, Clemens A. and De Boer, Jan and LaPointe, Vanessa Lydia Simone. The Components of Bone and What They Can Teach Us about Regeneration. *Materials* **2018**, 11.

- (55) Dave, H. D.; Shook, M.; Varacallo, M. Anatomy, Skeletal Muscle. In *StatPearls*, StatPearls Publishing Copyright © 2022, StatPearls Publishing LLC., 2022.
- (56) Langridge, B.; Griffin, M.; Butler, P. E. Regenerative medicine for skeletal muscle loss: a review of current tissue engineering approaches. *Journal of Materials Science: Materials in Medicine* **2021**, *32* (1). DOI: 10.1007/s10856-020-06476-5 (accessed 2022-07-07T17:00:00).
- (57) Zhang, W.; Liu, Y.; Zhang, H. Extracellular matrix: an important regulator of cell functions and skeletal muscle development. *Cell & Bioscience* **2021**, *11* (1). DOI: 10.1186/s13578-021-00579-4 (accessed 2022-04-13T17:34:14).
- (58) Kular, J. K.; Basu, S.; Sharma, R. I. The extracellular matrix: Structure, composition, age-related differences, tools for analysis and applications for tissue engineering. *Journal of Tissue Engineering* **2014**, *5* (0), 204173141455711. DOI: 10.1177/2041731414557112 (accessed 2022-04-12T22:15:28).
- (59) Lin, D. P. L.; Carnagarin, R.; Dharmarajan, A.; Dass, C. R. Transdifferentiation of myoblasts into osteoblasts – possible use for bone therapy. *Journal of Pharmacy and Pharmacology* **2017**, *69* (12), 1661-1671. DOI: 10.1111/jphp.12790 (accessed 2022-10-07T17:40:24).
- (60) Denes, L. T.; Riley, L. A.; Mijares, J. R.; Arboleda, J. D.; Mckee, K.; Esser, K. A.; Wang, E. T. Culturing C2C12 myotubes on micromolded gelatin hydrogels accelerates myotube maturation. *Skeletal Muscle* **2019**, *9* (1). DOI: 10.1186/s13395-019-0203-4 (accessed 2022-08-15T21:43:15).
- (61) McMahon, D. K.; Anderson, P. A.; Nassar, R.; Bunting, J. B.; Saba, Z.; Oakeley, A. E.; Malouf, N. N. C2C12 cells: biophysical, biochemical, and immunocytochemical properties. *Am J Physiol* **1994**, *266* (6 Pt 1), C1795-1802. DOI: 10.1152/ajpcell.1994.266.6.C1795 From NLM.
- (62) Niioka, H.; Asatani, S.; Yoshimura, A.; Ohigashi, H.; Tagawa, S.; Miyake, J. Classification of C2C12 cells at differentiation by convolutional neural network of deep learning using phase contrast images. *Human Cell* **2018**, *31* (1), 87-93. DOI: 10.1007/s13577-017-0191-9 (accessed 2022-03-08T07:36:20).

- (63) Zhang, Y.; Li, S.; Wen, X.; Tong, H.; Li, S.; Yan, Y. MYOC Promotes the Differentiation of C2C12 Cells by Regulation of the TGF- β Signaling Pathways via CAV1. *Biology* **2021**, *10* (7), 686. DOI: 10.3390/biology10070686.
- (64) Rosenfeld, S.; Schroeder, K.; Watkins-Castillo, S. The Economic Burden of Musculoskeletal Disease in Children and Adolescents in the United States. *Journal of pediatric orthopedics*: 2018; Vol. 38,4.
- (65) Langridge, B.; Griffin, M.; Butler, P. E. Regenerative medicine for skeletal muscle loss: a review of current tissue engineering approaches. *Journal of Materials Science-Materials in Medicine* **2021**, *32* (1). DOI: 10.1007/s10856-020-06476-5.
- (66) Kang, M. S.; Lee, S. H.; Park, W. J.; Lee, J. E.; Kim, B.; Han, D.-W. Advanced Techniques for Skeletal Muscle Tissue Engineering and Regeneration. *Bioengineering* **2020**, *7* (3), 99. DOI: 10.3390/bioengineering7030099 (accessed 2022-07-06T17:16:26).
- (67) O'Brien, F. J. Biomaterials & scaffolds for tissue engineering. *Materials Today* **2011**, *14* (3), 88-95. DOI: 10.1016/s1369-7021(11)70058-x (accessed 2022-05-16T23:21:23).
- (68) Nayak, T. R.; Andersen, H.; Makam, V. S.; Khaw, C.; Bae, S.; Xu, X. F.; Ee, P. L. R.; Ahn, J. H.; Hong, B. H.; Pastorin, G.; et al. Graphene for Controlled and Accelerated Osteogenic Differentiation of Human Mesenchymal Stem Cells. *Acs Nano* **2011**, *5* (6), 4670-4678. DOI: 10.1021/nn200500h.
- (69) Krueger, E.; Chang, A. N.; Brown, D.; Eixenberger, J.; Brown, R.; Rastegar, S.; Yocham, K. M.; Cantley, K. D.; Estrada, D. Graphene Foam as a Three-Dimensional Platform for Myotube Growth. *Acs Biomaterials Science & Engineering* **2016**, *2* (8), 1234-1241. DOI: 10.1021/acsbiomaterials.6b00139.

- (70) Frahs, S. M.; Reeck, J. C.; Yocham, K. M.; Frederiksen, A.; Fujimoto, K.; Scott, C. M.; Beard, R. S.; Brown, R. J.; Lujan, T. J.; Solov'yov, I. A.; et al. Prechondrogenic ATDC5 Cell Attachment and Differentiation on Graphene Foam; Modulation by Surface Functionalization with Fibronectin. *Acs Applied Materials & Interfaces* **2019**, *11* (45), 41906-41924. DOI: 10.1021/acsami.9b14670.
- (71) Yocham, K. M.; Scott, C.; Fujimoto, K.; Brown, R.; Tanasse, E.; Oxford, J. T.; Lujan, T. J.; Estrada, D. Mechanical Properties of Graphene Foam and Graphene Foam-Tissue Composites. *Advanced Engineering Materials* **2018**, *20* (9). DOI: 10.1002/adem.201800166.
- (72) Xie, H.; Cao, T.; Franco-Obregon, A.; Rosa, V. Graphene-Induced Osteogenic Differentiation Is Mediated by the Integrin/FAK Axis. *International Journal of Molecular Sciences* **2019**, *20* (3). DOI: 10.3390/ijms20030574.
- (73) Hernaez, M.; Zamarreno, C. R.; Melendi-Espina, S.; Bird, L. R.; Mayes, A. G.; Arregui, F. J. Optical Fibre Sensors Using Graphene-Based Materials: A Review. *Sensors* **2017**, *17* (1). DOI: 10.3390/s17010155. Feng, C.; Zhu, D.; Wang, Y.; Jin, S. J. Electromechanical Behaviors of Graphene Reinforced Polymer Composites: A Review. *Materials* **2020**, *13* (3). DOI: 10.3390/ma13030528. Bonaccorso, F.; Lombardo, A.; Hasan, T.; Sun, Z. P.; Colombo, L.; Ferrari, A. C. Production and processing of graphene and 2d crystals. *Materials Today* **2012**, *15* (12), 564-589. DOI: 10.1016/s1369-7021(13)70014-2. de Heer, W. A.; Berger, C.; Ruan, M.; Sprinkle, M.; Li, X. B.; Hu, Y. K.; Zhang, B. Q.; Hankinson, J.; Conrad, E. Large area and structured epitaxial graphene produced by confinement controlled sublimation of silicon carbide. *Proceedings of the National Academy of Sciences of the United States of America* **2011**, *108* (41), 16900-16905. DOI: 10.1073/pnas.1105113108.

- (74) Tang, B.; Guoxin, H.; Gao, H. Raman Spectroscopic Characterization of Graphene. *Applied Spectroscopy Reviews* **2010**, *45* (5), 369-407. DOI: 10.1080/05704928.2010.483886. No, Y.-S.; Choi, H. K.; Kim, J.-S.; Kim, H.; Yu, Y.-J.; Choi, C.-G.; Choi, J. S. Layer number identification of CVD-grown multilayer graphene using Si peak analysis. *Scientific Reports* **2018**, *8* (1). DOI: 10.1038/s41598-017-19084-1 (accessed 2022-07-25T16:08:40).
- (75) Lee, J.-U.; Yoon, D.; Cheong, H. Estimation of Young's Modulus of Graphene by Raman Spectroscopy. *Nano Letters* **2012**, *12* (9), 4444-4448. DOI: 10.1021/nl301073q (accessed 2022-05-10T17:05:52).
- (76) McMahon, D. K.; Anderson, P. A. W.; Nassar, R.; Bunting, J. B.; Saba, Z.; Oakeley, A. E.; Malouf, N. N. C2C12 CELLS - BIOPHYSICAL, BIOCHEMICAL, AND IMMUNOCYTOCHEMICAL PROPERTIES. *American Journal of Physiology* **1994**, *266* (6), C1795-C1802. DOI: 10.1152/ajpcell.1994.266.6.C1795. Denes, L. T.; Riley, L. A.; Mijares, J. R.; Arboleda, J. D.; McKee, K.; Esser, K. A.; Wang, E. T. Culturing C2C12 myotubes on micromolded gelatin hydrogels accelerates myotube maturation. *Skeletal Muscle* **2019**, *9*. DOI: 10.1186/s13395-019-0203-4.
- (77) Wang, L.; Wu, Y.; Guo, B.; Ma, P. Nanofiber Yarn/Hydrogel Core-Shell Scaffolds Mimicking Native Skeletal Muscle Tissue for Guiding 3D Myoblast Alignment, Elongation, and Differentiation. *ACS nano* **2015**, *9*. DOI: 10.1021/acsnano.5b03644.
- (78) Morrill, E. E.; Tulepbergenov, A. N.; Stender, C. J.; Lamichhane, R.; Brown, R. J.; Lujan, T. J. A validated software application to measure fiber organization in soft tissue. *Biomechanics and Modeling in Mechanobiology* **2016**, *15* (6), 1467-1478. DOI: 10.1007/s10237-016-0776-3 (accessed 2022-05-17T16:00:23).
- (79) Wang, Y.; Zheng, Y.; Xu, X.; Dubuisson, E.; Bao, Q.; Lu, J.; Loh, K. P. Electrochemical Delamination of CVD-Grown Graphene Film: Toward the Recyclable Use of Copper Catalyst. *ACS Nano* **2011**, *5* (12), 9927-9933. DOI: 10.1021/nn203700w (accessed 2022-06-06T17:17:13).

- (80) Williams- Godwin, L.; Brown, D.; Livingston, R.; Webb, T.; Karriem, L.; Graugnard, E.; Estrada, D. Open-source automated chemical vapor deposition system for the production of two- dimensional nanomaterials. *PLOS ONE* **2019**, *14* (1), e0210817. DOI: 10.1371/journal.pone.0210817 (accessed 2022-06-06T17:27:44).
- (81) Pandhi, T.; Kreit, E.; Aga, R.; Fujimoto, K.; Sharbati, M. T.; Khademi, S.; Chang, A. N.; Xiong, F.; Koehne, J.; Heckman, E. M.; et al. Electrical Transport and Power Dissipation in Aerosol-Jet-Printed Graphene Interconnects. *Scientific Reports* **2018**, *8* (1). DOI: 10.1038/s41598-018-29195-y (accessed 2022-06-06T17:47:04).
- (82) Bateman, A.; Martin, M.-J.; Orchard, S.; Magrane, M.; Agivetova, R.; Ahmad, S.; Alpi, E.; Bowler-Barnett, E. H.; Britto, R.; Bursteinas, B.; et al. UniProt: the universal protein knowledgebase in 2021. *Nucleic Acids Research* **2021**, *49* (D1), D480-D489. DOI: 10.1093/nar/gkaa1100 (accessed 2021-12-22T15:44:33).
- (83) Paulin, D.; Li, Z. Desmin: a major intermediate filament protein essential for the structural integrity and function of muscle. *Exp Cell Res* **2004**, *301* (1), 1-7. DOI: 10.1016/j.yexcr.2004.08.004 From NLM.
- (84) Harmon, E. B.; Harmon, M. L.; Larsen, T. D.; Paulson, A. F.; Perryman, M. B. Myotonic dystrophy protein kinase is expressed in embryonic myocytes and is required for myotube formation. *Developmental dynamics: an official publication of the American Association of Anatomists* **2008**, *237* (9), 2353-2366.
- (85) Herbst, R. MuSk function during health and disease. *Neurosci Lett* **2020**, *716*, 134676. DOI: 10.1016/j.neulet.2019.134676 From NLM.
- (86) Miller, J. B. Myogenic programs of mouse muscle cell lines: expression of myosin heavy chain isoforms, MyoD1, and myogenin. *Journal of Cell Biology* **1990**, *111* (3), 1149-1159. Mohammadabadi, M.; Bordbar, F.; Jensen, J.; Du, M.; Guo, W. Key Genes Regulating Skeletal Muscle Development and Growth in Farm Animals. *Animals* **2021**, *11* (3), 835. DOI: 10.3390/ani11030835.

- (87) Ganassi, M.; Badodi, S.; Wanders, K.; Zammit, P. S.; Hughes, S. M. Myogenin is an essential regulator of adult myofibre growth and muscle stem cell homeostasis. *eLife* **2020**, *9*, e60445. DOI: 10.7554/eLife.60445.
- (88) Gramolini, A. O.; Jasmin, B. J. Expression of the utrophin gene during myogenic differentiation. *Nucleic acids research* **1999**, *27* (17), 3603-3609.
- (89) Park, J.-W.; Lee, J. H.; Kim, S. W.; Han, J. S.; Kang, K. S.; Kim, S.-J.; Park, T. S. Muscle differentiation induced up-regulation of calcium-related gene expression in quail myoblasts. *Asian-Australasian journal of animal sciences* **2018**, *31* (9), 1507.
- (90) Nakayama, M.; Stauffer, J.; Cheng, J.; Banerjee-Basu, S.; Wawrousek, E.; Buonanno, A. Common core sequences are found in skeletal muscle slow-and fast-fiber-type-specific regulatory elements. *Molecular and Cellular Biology* **1996**, *16* (5), 2408-2417.
- (91) Lewis, M.; Tippet, H.; Sinanan, A.; Morgan, M.; Hunt, N. Gelatinase-B (matrix metalloproteinase-9; MMP-9) secretion is involved in the migratory phase of human and murine muscle cell cultures. *Journal of Muscle Research & Cell Motility* **2000**, *21* (3), 223-233.
- (92) Hoegy, S. E.; Oh, H. R.; Corcoran, M. L.; Stetler-Stevenson, W. G. Tissue inhibitor of metalloproteinases-2 (TIMP-2) suppresses TKR-growth factor signaling independent of metalloproteinase inhibition. *J Biol Chem* **2001**, *276* (5), 3203-3214. DOI: 10.1074/jbc.M008157200 From NLM.